

Current status of the light neutralino thermal dark matter in the phenomenological MSSM

Rahool Kumar Barman,^{1,*} Genevieve Bélanger,^{2,†}
 Biplob Bhattacharjee,^{3,‡} Rohini Godbole^{a†,3,§} and Rhitaja Sengupta^{4,¶}

¹*Kavli IPMU (WPI), UTIAS, The University of Tokyo, Kashiwa, Chiba 277-8583, Japan*

²*LAPTh, Université Savoie Mont Blanc, CNRS, B.P. 110, F-74941 Annecy Cedex, France*

³*Centre for High Energy Physics, Indian Institute of Science, Bangalore 560012, India*

⁴*Bethe Center for Theoretical Physics and Physikalisches Institut der Universität Bonn, Nußallee 12, 53115 Bonn, Germany*

In a previous publication, we studied the parameter space of the phenomenological Minimal Supersymmetric Standard Model (pMSSM) with a light neutralino thermal dark matter ($M_{\tilde{\chi}_1^0} \leq M_h/2$) and observed that the recent results from the dark matter and collider experiments put strong constraints on this scenario. In this work, we present in detail the arguments behind the robustness of this result against scanning over the large number of parameters in pMSSM. The Run-3 of LHC will be crucial in probing the surviving regions of the parameter space. We further investigate the impact of light staus on our parameter space and also provide benchmarks which can be interesting for Run-3 of LHC. We analyse these benchmarks at the LHC using the machine learning framework of XGBOOST. Finally, we also discuss the effect of non-standard cosmology on the parameter space.

I. INTRODUCTION

Since the discovery of the 125 GeV Higgs boson (h) by the ATLAS and CMS collaborations in 2012, the precise quantification of its non-standard couplings has been a major cornerstone of the new physics search program at the LHC. Until now, clear evidence of physics beyond the Standard Model (SM) is yet to be observed at the LHC. Within experimental uncertainties, measurements indicate that the observed properties of h are consistent with the expectations for the SM Higgs boson. While the couplings of the Higgs boson with the third-generation charged fermions and gauge bosons have been measured with considerable precision, uncertainties in the second-generation Yukawa coupling measurements are gradually reducing with improved statistics. Nonetheless, the current data still allow non-standard decays for the discovered Higgs boson. An exciting aspect of non-standard interactions of Higgs bosons is their decay into an invisible final state. Recent analyses of the LHC Run-II data by the ATLAS and CMS collaborations have constrained the branching fraction for Higgs invisible decay to 11% [1] and 15% [2] at 95% CL, respectively. The invisible final states can be dark matter (DM) candidates, as long as they are stable or have a lifetime larger than the age of the Universe, thus transmuting Higgs invisible searches at the LHC to potential probes for the elusive Dark Matter.

^a † Deceased. *Sadly, our distinguished colleague Rohini Godbole passed away while this work was being finalized. She will be missed.*

* rahool.barman@ipmu.jp

† belanger@lapth.cnrs.fr

‡ biplob@iisc.ac.in

§ rohini@iisc.ac.in

¶ rsengupt@uni-bonn.de

The R-parity conserving (RPC) Minimal Supersymmetric Standard Model (MSSM), with no explicit terms for baryon number and lepton number violation, provides a stable lightest supersymmetric particle (LSP), typically the neutralino $\tilde{\chi}_1^0$, which can be a WIMP (weakly interacting massive particle) DM candidate. Charged under the $SU(2)_L \times U(1)_Y$ gauge group, the LSP neutralino can typically generate the correct relic abundances at a mass of $\mathcal{O}(100)$ GeV, making it one of the most favorable and widely studied cold DM candidates. It is also worth noting that the MSSM can address the “naturalness” problem [3–5] while also accommodating a scalar boson consistent with the h measurements, thus remaining one of the most attractive frameworks to pursue new physics beyond the scope of the Standard Model.

In this paper, we focus on the case of a light neutralino DM with mass $M_{\tilde{\chi}_1^0} \leq M_h/2$ such that the Higgs boson can decay invisibly through $h \rightarrow \tilde{\chi}_1^0 \tilde{\chi}_1^0$. Since charged Higgsinos and Winos are constrained to have masses above $\gtrsim 100$ GeV by LEP searches [6, 7], the $\tilde{\chi}_1^0$ with mass below $\lesssim M_h/2$ is left with the sole possibility of a dominant Bino admixture. The observed DM abundance in our Universe is $\Omega_{DM}^{obs} h^2 = 0.120 \pm 0.001$ as measured by the PLANCK collaboration [8]. However, the annihilation cross-section for Bino-dominated neutralinos is too small and leads to overclosure of the Universe ($\Omega_{LSP} h^2 > \Omega_{DM}^{obs} h^2$), except under special circumstances, such as annihilation through an s -channel resonance with a mass of $\sim 2M_{\tilde{\chi}_1^0}$ and sfermion exchange. Our primary focus in this work will be the first scenario, however, we will also study the implications of light sfermions on our results. When the LSP contributes to the invisible decay of the SM-like Higgs boson, the available resonances through which it can annihilate are the Z and h bosons. The regions of parameter space where the LSP mass lies within a window of 3-5 GeV around half the Z boson mass (45 GeV) or half the h boson mass (62.5 GeV), are referred to as the Z funnel region or the h funnel region, respectively.

Several studies have explored the prospect of a light neutralino DM, in the constrained MSSM (cMSSM) and the phenomenological MSSM (pMSSM) considering the various experimental constraints at the time [9–47]. The ATLAS and CMS Collaborations at the LHC have made available new results from searches of heavy Higgs bosons [48], direct searches of charginos and neutralinos (collectively known as electroweakinos) [49–52], as well as the invisible decay of the SM Higgs boson [53] at Run2. The XENON-1T, XENON-nT, PICO-60, PandaX-4T, and LUX-ZEPLIN (LZ) collaborations have also published limits on the DM direct detection (DD) cross-sections – both spin-dependent (SD) and spin-independent (SI) [54–60]. Among these, the results from the LZ collaboration provide the most stringent bounds on the SI DD cross-sections [58] for DM masses in the 10 GeV - 1 TeV range. With these new and improved results, revisiting the MSSM parameter space containing light neutralino DM, which can also contribute to the invisible decay of the Higgs boson, becomes crucial.

In Ref. [47], we investigated the current status of the pMSSM parameter space with ten free parameters, that accommodates a light neutralino DM satisfying the upper bound on the relic density, with Higgsino-like NLSP. We considered both positive and negative values for the Higgsino mass parameter μ . The implications from the latest direct detection experiments in both spin-independent and spin-dependent interactions were studied in conjunction with the current bounds from Higgs invisible measurements, heavy Higgs searches as well as electroweakino searches at the LHC. We found that the latest direct detection limit from the LZ collaboration puts the $\mu > 0$ scenario under severe tension. For the $\mu < 0$ scenario, the LZ bound along with the constraints from electroweakino searches at colliders exclude most of the parameter space, except for very light Higgsinos, having masses 125 – 145 GeV and 145 – 160 GeV in the Z and h funnel regions, respectively.

In this paper, we present comprehensive and exhaustive arguments for the results found in Ref. [47]. To further concretise our findings, we study the interplay of direct detection and collider limits in a simplified scenario consisting of the SM extended by a spin-1/2 Majorana fermion DM in analogy with the neutralino $\tilde{\chi}_1^0$ DM in the pMSSM framework. We then investigate the light Higgsinos surviving in the negative μ scenario and the current analyses sensitive to them. We choose benchmarks from the different allowed regions of our parameter space and perform a dedicated analysis of the $3l + \cancel{E}_T$ channel for light Higgsinos in the $\mu < 0$ scenario using a machine learning algorithm, XGBOOST, to explore its potential sensitivity. We further extend our previous work to study the impact of light staus. We present benchmarks where the Higgsino can decay to staus and perform an analysis with tau leptons in the final

state to explore the sensitivity for Run-3. Finally, we discuss how the status changes for a thermal neutralino in non-standard cosmological scenarios.

We organise this paper as follows: In Sec. II, we summarize the Higgs and electroweakino sectors of the MSSM, most relevant to the present analysis. The parameter space of interest, scanning technique and the scan ranges, are also discussed in the same section. The impact of constraints from LEP measurements, flavor observables, and Higgs measurements at the LHC, is examined in Sec. III. We devote Sec. IV to exploring the implications from relic density bounds. The effect of constraints from direct detection measurements on the Z and h funnel regions are scrutinized in Sec. IV A and IV B. Sec. IV C examines a simplified scenario with the SM extended by a stable Majorana fermion. We discuss the effect of electroweakino constraints in Sec. V. Details and results from our collider analysis targeted on smaller Higgsino mass $\mu \lesssim 160$ GeV are presented in Sec. VI. In Sec. VII and Sec. VIII, we respectively discuss how our results change when we have light staus and in scenarios of non-standard cosmology. We conclude in Sec. IX.

II. THE pMSSM FRAMEWORK AND THE PARAMETER SPACE

In the pMSSM framework, the lightest neutralino $\tilde{\chi}_1^0$ is a well-motivated DM candidate, provided it is the LSP. The $\tilde{\chi}_1^0$ eigenstate can be written in terms of the Bino (\tilde{B}), neutral Wino (\tilde{W}_3) and neutral Higgsinos (\tilde{H}_1^0 and \tilde{H}_2^0),

$$\tilde{\chi}_1^0 = N_{11}\tilde{B} + N_{12}\tilde{W}^3 + N_{13}\tilde{H}_1^0 + N_{14}\tilde{H}_2^0, \quad (1)$$

where, N_{1i} represents the amount of Bino ($i = 1$), Wino ($i = 2$) and the Higgsino ($i = 3, 4$) admixtures. In the present work, we are interested in the region of the pMSSM parameter space where $\tilde{\chi}_1^0$ is the LSP and ‘light’, i.e., $M_{\tilde{\chi}_1^0} \leq M_h/2$, such that it is kinematically feasible for the SM-like Higgs boson h to decay into a pair of $\tilde{\chi}_1^0$ ’s, thus contributing to its invisible decay. $\tilde{\chi}_1^0$ interacts with other electroweakinos via the exchange of SM Z/W^\pm bosons and the pMSSM Higgs bosons, with the coupling strengths determined by their electroweakino composition. These various interactions of the LSP become important factors in the calculation of its relic density and direct detection cross-sections. The $\tilde{\chi}_1^0\tilde{\chi}_1^0Z$ coupling can be expressed as follows [61],

$$g_{\tilde{\chi}_1^0\tilde{\chi}_1^0Z}^L = -\frac{g}{2\cos\theta_W} (|N_{13}|^2 - |N_{14}|^2), \quad g_{\tilde{\chi}_1^0\tilde{\chi}_1^0Z}^R = -g_{\tilde{\chi}_1^0\tilde{\chi}_1^0Z}^L, \quad (2)$$

where g is the SU(2) gauge coupling, θ_W is the Weinberg angle, and L, R denotes the respective couplings with the left and right-handed $\tilde{\chi}_1^0$. Similarly, the coupling of $\tilde{\chi}_1^0$ with the three neutral Higgs bosons of the MSSM Higgs sector can be expressed as [61]:

$$g_{\tilde{\chi}_1^0\tilde{\chi}_1^0(h/H/A)}^L = g(N_{12} - \tan\theta_W N_{11})(e_{h/H/A}N_{13} + d_{h/H/A}N_{14}), \\ g_{\tilde{\chi}_1^0\tilde{\chi}_1^0(h/H)}^R = g_{\tilde{\chi}_1^0\tilde{\chi}_1^0(h/H)}^L, \quad g_{\tilde{\chi}_1^0\tilde{\chi}_1^0A}^R = -g_{\tilde{\chi}_1^0\tilde{\chi}_1^0A}^L, \quad (3)$$

where,

$$e_h = -\sin\alpha, \quad e_H = \cos\alpha, \quad e_A = -\sin\beta, \\ d_h = -\cos\alpha, \quad d_H = -\sin\alpha, \quad d_A = \cos\beta, \quad (4)$$

where α is the mixing angle in the CP-even neutral Higgs sector and $\tan\beta$ is the ratio of the vacuum expectation values (*vevs*) of the two Higgs doublets.

We require the light CP-even neutral Higgs boson h to be consistent with the properties of the observed SM-like Higgs boson. h can decay via $h \rightarrow \tilde{\chi}_1^0\tilde{\chi}_1^0$, provided $M_{\tilde{\chi}_1^0} \leq M_h/2$ and $|g_{\tilde{\chi}_1^0\tilde{\chi}_1^0h}| > 0$. As previously discussed, the former condition requires a Bino-dominated $\tilde{\chi}_1^0$ in order to evade the lower bounds on $M_{\tilde{\chi}_1^\pm}$ from LEP measurements [7]. We also notice from Eqn. 3 that $g_{\tilde{\chi}_1^0\tilde{\chi}_1^0h}$ becomes zero when $\tilde{\chi}_1^0$ is a pure Gaugino, referred to Bino and Wino collectively, or a pure Higgsino. Therefore, a Gaugino-dominated $\tilde{\chi}_1^0$ must have some Higgsino admixture to couple with the SM-like Higgs boson, which typically entails a dominant Higgsino-like next-to-lightest supersymmetric particle (NLSP).

Furthermore, the lower bounds on the masses of Higgsinos are less stringent than that of the Winos. Accordingly, in the present study, we are led to the parameter space where $\tilde{\chi}_2^0$, $\tilde{\chi}_3^0$ and $\tilde{\chi}_1^\pm$ have a predominant Higgsino composition, while $\tilde{\chi}_4^0$ and $\tilde{\chi}_2^\pm$ have a dominant Wino admixture.

Additionally, $\tilde{\chi}_1^0$ interacts with the SM fermions and sfermions. Searches at the LHC have derived strong lower bounds on the first two generations of squarks. For example, a single non-degenerate squark is constrained above $\gtrsim 1200$ GeV for $M_{\tilde{\chi}_1^0} \sim 60$ GeV [62]. Therefore, the effect of their interactions on the observables related to the LSP will be negligible and motivates fixing their mass parameters to high values, say 5 TeV.

The sleptons are relatively weakly constrained from collider searches and their couplings with $\tilde{\chi}_1^0$ can be expressed as [61],

$$g_{\tilde{\chi}_1^0 \tilde{l} \bar{l}} = \sqrt{2} g \sin \theta_W \left[Q_l (N_{11} \cos \theta_W + N_{12} \sin \theta_W) + (I_l^3 - Q_l \sin^2 \theta_W) \frac{N_{12} \cos \theta_W - N_{11} \sin \theta_W}{\cos \theta_W \sin \theta_W} \right], \quad (5)$$

where Q_l and I_l^{3j} are the charge of the lepton and the third component of isospin of the lepton, respectively. Among the three generations of sleptons, the staus have the weakest limits from collider searches. Therefore, the presence of light staus can impact the parameter space of light neutralino thermal DM. We perform our scan in two parts – without and with light staus.

The relevant input parameters are: the Gaugino masses, M_1 (Bino) and M_2 (Wino), the Higgsino mass parameter μ , the ratio of the Higgs vacuum expectation values $\tan \beta$, the pseudoscalar mass M_A , the mass of the third generation squarks $\{M_{\tilde{Q}_{3L}}, M_{\tilde{t}_R}, M_{\tilde{b}_R}\}$, the trilinear coupling of the stop, A_t , and the gluino mass parameter, M_3 . We perform a random scan over these ten input parameters in the ranges specified below:

$$\begin{aligned} 30 \text{ GeV} < M_1 < 100 \text{ GeV}, \quad 1 \text{ TeV} < M_2 < 3 \text{ TeV}, \\ 100 \text{ GeV} < |\mu| < 2 \text{ TeV}, \\ 2 < \tan \beta < 50, \quad 100 \text{ GeV} < M_A < 6 \text{ TeV}, \\ 3 \text{ TeV} < M_{\tilde{Q}_{3L}} < 20 \text{ TeV}, \quad 3 \text{ TeV} < M_{\tilde{t}_R} < 20 \text{ TeV}, \\ 3 \text{ TeV} < M_{\tilde{b}_R} < 20 \text{ TeV}, \quad -20 \text{ TeV} < A_t < 20 \text{ TeV}, \\ 2 \text{ TeV} < M_3 < 5 \text{ TeV}. \end{aligned} \quad (6)$$

For the first part of the scan, i.e., without the light staus, we decouple the first two generations of squarks and all the three generations of sleptons from the spectrum and set the following pMSSM input parameters to a fixed value,

$$\begin{aligned} M_{\tilde{Q}_{1,2L}} = M_{\tilde{u}_{1,2R}} = M_{\tilde{d}_{1,2R}} = 5 \text{ TeV}, \quad A_{u/d/c/s/b} = 0, \\ M_{\tilde{L}_{1,2,3L}} = M_{\tilde{e}_{1,2,3R}} = 2 \text{ TeV}, \quad A_{e/\mu/\tau} = 0. \end{aligned} \quad (7)$$

Here, $\{M_{\tilde{Q}_{1,2L}}, M_{\tilde{u}_{1,2R}}, M_{\tilde{d}_{1,2R}}\}$ are the first and second generation squark mass parameters, and $\{M_{\tilde{L}_{1,2,3L}}, M_{\tilde{e}_{1,2,3R}}\}$ are the left and right-handed slepton mass parameters.

We perform separate scans for the positive and negative values of μ to examine the role of $\text{sgn}(\mu)$ on the results. It is also worth noting that within the parameter space of our interest, DM relic density and direct detection constraints restrict $M_{\tilde{\chi}_1^0}$ to the Z and h funnel regions only [45, 46, 63]. We begin by performing a random scan over the specified parameter space. Subsequently, in order to sufficiently populate the funnel regions, we perform a dedicated scan where we dynamically tune M_1 such that $M_{\tilde{\chi}_1^0}$ is within $M_Z/2 \pm 5$ GeV or $M_h/2 \pm 3$ GeV, where M_h is the mass of the Higgs boson estimated by `FeynHiggs` for each point in the parameter space. Additionally, we extract the pole mass of the top quark, M_t , randomly from a gaussian distribution with a central value of 173.21 GeV and a standard deviation of 0.55 GeV [64]¹

¹ Note that using the more recent measured value of $M_t = 172.69$ GeV [65] does not affect our final results, since it is always possible to adjust the stop mass parameters, which we scan over, to obtain the measured value of the Higgs boson mass.

To study the effect of light staus, we perform a second scan where we vary the stau mass parameters, in a way that the staus become the NLSPs. We can accommodate single left-handed (LH) or right-handed (RH) staus with masses around 100-150 GeV according to Ref. [66]. According to Eqn. 5, the coupling of sleptons with the LSP neutralino depends on the third component of isospin of the slepton, which is higher for RH staus as compared to the LH ones. Therefore, RH staus will have greater impact on the relic density. To avoid constraints from additional light LH staus and light sneutrino, we consider only light RH staus. This is a minimal extension to our earlier scan [47], which is achieved by lowering the parameter $M_{\tilde{e}_{3R}}$, and varying it between 85 GeV and 500 GeV, while keeping $M_{\tilde{L}_{3L}}$ and A_τ fixed at 2 TeV and 0, respectively.

We use `FeynHiggs 2.18.1` [67–74] to generate the particle spectrum of the SUSY particles and of the Higgs bosons for each set of input parameters² and branching fractions for the decay of the Higgs bosons. `MicrOMEGAS 5.2.13` [75–80] is used to compute the LEP, flavor physics, and dark matter observables, as further discussed in Sec. III, where we also describe the various relevant constraints and their impact on the scanned parameter space.

III. CONSTRAINTS FROM LEP, FLAVOR OBSERVABLES AND THE HIGGS SECTOR

As previously discussed, we associate the lightest CP-even Higgs boson h with the discovered Higgs boson at the LHC, and require that the masses and branching of the two match within experimental and theoretical uncertainties. Measurements at the LHC have put the mass of the Higgs boson at 125.38 ± 0.14 GeV [81]. We require that the mass of h , as computed by `FeynHiggs 2.18.1`, be in the range 122 GeV – 128 GeV. Considering theoretical uncertainties stemming from the dependence on the renormalisation scheme and scale, from the assumption of zero external momentum in two-loop corrections, and also absence of higher order corrections, we allow for a conservative 3 GeV window around the experimentally measured value [82–84]³. At low values of $\tan\beta$, consistency with the Higgs boson mass constraint requires large A_t and stop masses. However, large A_t can give rise to color and charge-breaking minima (CCB) [85–87], where the scalar partners of top quarks having color and electric charges develop a non-zero vev and the corresponding minima is lower than the minima of the Higgs field. This can be evaded, given, $|X_t| < \sqrt{6M_{t_1}M_{t_2}}$ [86], where $X_t = A_t - \mu/\tan\beta$ and $M_{t_{1,2}}$ represents the stop masses. In the present study, we see that the CCB condition has no significant effect on the allowed parameter space.

We also apply limits on the invisible decay width of Z -boson $\Gamma_Z \leq 2$ MeV [88], chargino mass $M_{\tilde{\chi}_1^0} \geq 103.5$ GeV [7], and cross-section of neutralino pair production $\sigma(\tilde{\chi}_2^0\tilde{\chi}_1^0) \leq 0.1$ pb in final states with jets + \cancel{E}_T [7], as obtained from LEP. We impose constraints on various flavor physics observables, such as, $Br(b \rightarrow s\gamma) = (3.32 \pm 0.16) \times 10^{-4}$ [89], $Br(B_s \rightarrow \mu^+\mu^-) = 3.0_{-0.63}^{+0.67} \times 10^{-9}$ [90], and $Br(B \rightarrow \tau\nu) = 1.28 \pm 0.25$ [91], allowing 2σ uncertainty around the best-fit values. We have used `MicrOMEGAS 5.2.13` [75–80] to calculate both the LEP and flavor physics observables.

We also impose the Higgs signal strength constraints on the parameter space using the `HiggsSignal 2.6.2` [92–94] package, while limits from the heavy Higgs boson searches at the LHC are imposed using the `HiggsBounds 2.10.0` [95–99] package. The parameter space is also required to satisfy the most stringent upper bound on the Higgs invisible branching ratio $Br(h \rightarrow \text{inv}) \leq 11\%$, as measured by the ATLAS collaboration [1], which is stronger than the current CMS bound (15% [2]). Hereafter, constraints on the mass, signal strength (imposed through `HiggsSignal 2.6.2`), and the invisible branching ratio of the Higgs boson are collectively referred to as the constraints on ‘‘Higgs properties’’. We summarize the constraints in Table I.

We show the scanned points in the $M_A - \tan\beta$ plane for $\mu > 0$ (top) and $\mu < 0$ (bottom) and the effect of various constraints in Fig. 1. In the left panels, we show the parameter points allowed by the Higgs boson measurements and

² The input parameters are read and written in the SLHA file as on-shell parameters by the `FeynHiggs` code. We find no significant changes in our result when we use a different spectrum generator, such as `SoftSUSY-4.1.17`, which provides the output SLHA with \overline{DR} parameters.

³ Additionally, we can compute the error in estimating the mass of the Higgs boson using `FeynHiggs 2.18.1`, denoted as $\Delta_{M_h}^{FH}$. We discuss in a later section the impact of a precise Higgs mass condition, defined as requiring $M_h \pm \Delta_{M_h}^{FH} \in [125.38 - 2 \times 0.14 \text{ GeV}, 125.38 + 2 \times 0.14 \text{ GeV}]$, i.e., within 2σ of the experimentally measured mass of the Higgs boson.

Sr. No.	Observable	Calculated by	Constraint
(1)	Light Higgs boson mass	FeynHiggs 2.18.1	$122 \text{ GeV} < M_h < 128 \text{ GeV}$
(2)	Higgs signal strength	HiggsSignal 2.6.2	111 channels, $p\text{-value} > 0.05$
(3)	Heavy Higgs bosons	HiggsBounds 2.10.0	Constraints from collider searches of heavy Higgs bosons implemented in HiggsBounds
(4)	Invisible decay of Higgs boson	FeynHiggs 2.18.1	$\text{Br}(h \rightarrow \tilde{\chi}_1^0 \tilde{\chi}_1^0) < 0.11$
(5)	Invisible decay of Z boson from LEP	MicrOMEGAS 5.2.13	$\Gamma(Z \rightarrow \text{invisible}) < 2 \text{ MeV}$
(6)	Chargino mass limit from LEP	FeynHiggs 2.18.1	$M_{\tilde{\chi}_1^\pm} > 103 \text{ GeV}$
(7)	LEP limits on neutralino in dijet + MET final states	MicrOMEGAS 5.2.13	$\sigma(e^+e^- \rightarrow \tilde{\chi}_1^0 \tilde{\chi}_2^0) \times \text{Br}(\tilde{\chi}_2^0 \rightarrow \tilde{\chi}_1^0 + \text{jets}) +$ $\sigma(e^+e^- \rightarrow \tilde{\chi}_1^0 \tilde{\chi}_3^0) \times \text{Br}(\tilde{\chi}_3^0 \rightarrow \tilde{\chi}_1^0 + \text{jets}) <$ 0.1 pb
(8)	Flavour observables	MicrOMEGAS 5.2.13	$3.00 \times 10^{-4} < \text{Br}(b \rightarrow s\gamma) < 3.64 \times 10^{-4}$ $1.66 \times 10^{-9} < \text{Br}(B_s \rightarrow \mu^+ \mu^-) < 4.34 \times 10^{-9}$ $0.78 < \frac{(\text{Br}(B \rightarrow \tau\nu))_{\text{obs}}}{(\text{Br}(B \rightarrow \tau\nu))_{\text{SM}}} < 1.78$

TABLE I. Summary of constraints from Higgs sector, LEP, and flavor observables.

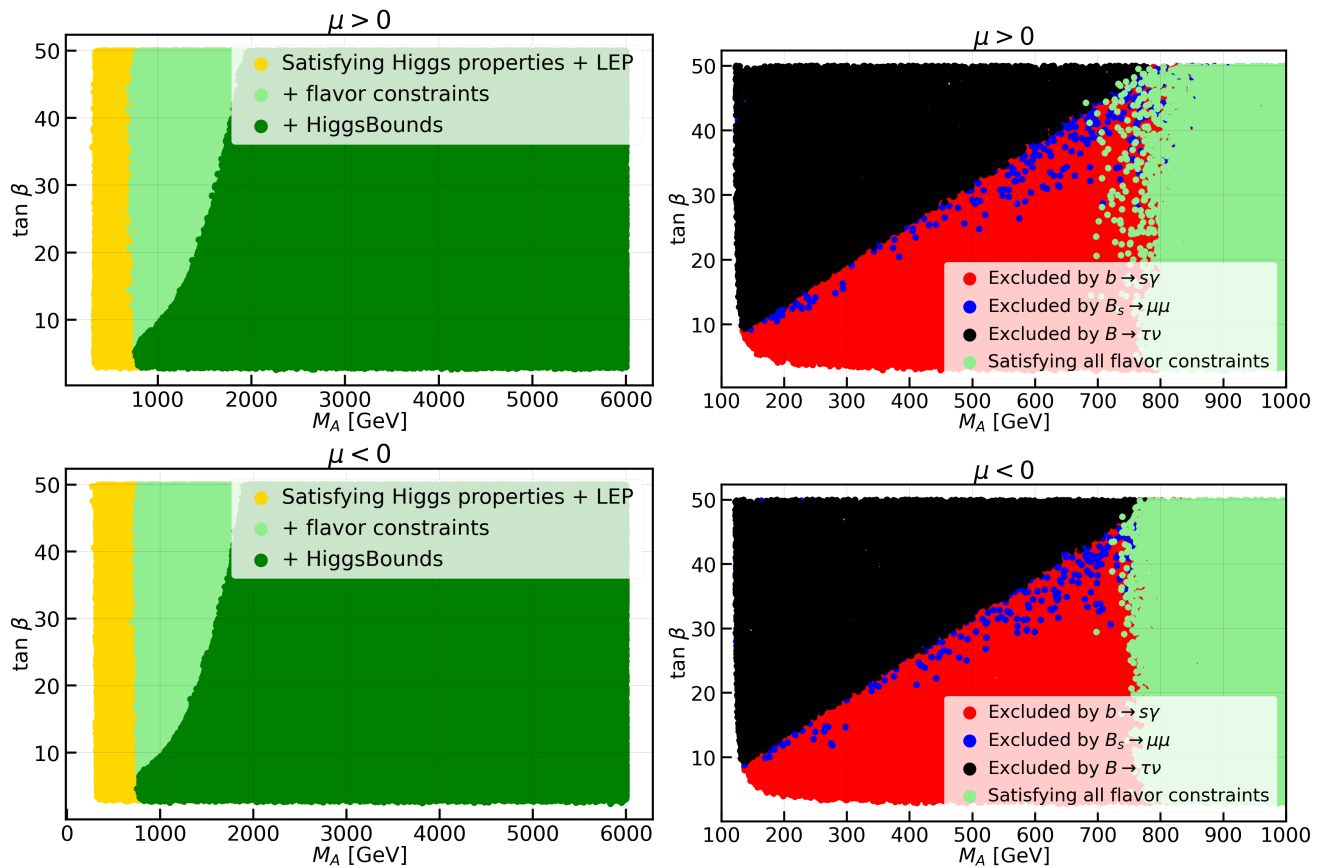


FIG. 1. *Left*: Parameter space in the M_A - $\tan\beta$ plane satisfying the Higgs properties, LEP constraints, flavor constraints, and results of heavy Higgs boson searches implemented in **HiggsBounds**; *Right*: Parameter space in the M_A - $\tan\beta$ plane zoomed-in to show the effect of the different flavor observables for $M_A < 1 \text{ TeV}$. The *top* and *bottom* panels are for $\mu > 0$ and $\mu < 0$ respectively.

LEP constraints (yellow), flavor physics bounds (light-green), and the constraints from heavy Higgs searches included via **HiggsBounds** (dark-green), applied consecutively. In the right panels, we zoom in on the $M_A \leq 1 \text{ TeV}$ region,

showing the parameter space excluded by different flavor-changing processes. The flavor physics observables together exclude points with low M_A ($\lesssim 700$ GeV). The low $\tan\beta$ region is excluded by $Br(b \rightarrow s\gamma)$ while the other two flavor observables are more impacting in the high $\tan\beta$ region. Points in the high $\tan\beta$ region for $700 \text{ GeV} \lesssim M_A \lesssim 2 \text{ TeV}$ are excluded by constraints from heavy Higgs boson searches at the LHC applied via the `HiggsBounds` package. Among the various heavy Higgs searches considered, results from the search for heavy Higgs bosons decaying into a pair of tau leptons at $\sqrt{s} = 13 \text{ TeV}$ with $\mathcal{L} = 139 \text{ fb}^{-1}$ data [48] by the ATLAS collaboration resulted in the most stringent constraints on the parameter space of our interest. We further observe that the LEP constraints (Table I (2), (3), and (4) applied together), `HiggsSignal` and the upper limit on the invisible branching of h to invisible final states do not show any specific trend in excluding the parameter space in the M_A - $\tan\beta$ plane. All these observations are irrespective of the sign of the μ parameter.

IV. DARK MATTER CONSTRAINTS

As discussed previously, the lightest supersymmetric particle in the pMSSM, here $\tilde{\chi}_1^0$, is a viable DM candidate. It can have a thermal production in the early Universe, which freezes-out. In the standard cosmology, we require the relic density of the LSP $\Omega_{\tilde{\chi}_1^0}$ to be equal to the observed DM relic density as measured by the PLANCK collaboration $\Omega_{DM}^{obs} h^2 = 0.120 \pm 0.001$ [100], which assuming a 2σ interval can vary from $0.118 \lesssim \Omega_{DM}^{obs} h^2 \lesssim 0.122$. Lifting up the requisite that the neutralino LSP forms 100% of the observed DM relic owing to the possibility of multicomponent DM, we can modify the relic density constraint to $\Omega_{\tilde{\chi}_1^0} \lesssim 0.122$. We use the `MicrOMEGAS 5.2.13` [75–80, 101] package to compute the relic density of $\tilde{\chi}_1^0$.

In addition to the relic density constraint, we need to take into consideration the limits from dark matter direct detection (DD) experiments which constrain the spin-dependent DM-neutron (SDn), DM-proton (SDp) and spin-independent (SI) DM-nucleon interaction cross-sections as a function of mass of the DM. We use `MicrOMEGAS 5.2.13` to compute these cross-sections and then compare them with the 90% confidence level (CL) upper limits quoted by the PICO-60 (SDp [56]), PandaX-4T (SDn [59]), and LZ (SI [58]) experiments, since these are the strongest available bounds for each category in the DM mass range of 10 GeV to 1 TeV at present. The LZ collaboration sets an upper limit on the SI cross-section of a DM particle with mass in the Z -funnel to be $1.06 \times 10^{-47} \text{ cm}^2$, and in the h -funnel to be $1.54 - 1.64 \times 10^{-47} \text{ cm}^2$ for $M_h \in 122 - 128 \text{ GeV}$. We tabulate the DM related constraints applied on the parameter space of our interest in Table II.

Sr. No.	Observable	Calculated by	Constraint
(9)	Relic density	<code>MicrOMEGAS 5.2.13</code>	$\Omega < 0.122$ (PLANCK)
(10)	Limits on direct detection cross-sections scaled with ξ (Eqn. 8)	<code>MicrOMEGAS 5.2.13</code>	Spin-dependent proton: PICO-60 Spin-dependent neutron: PandaX-4T Spin-independent: LUX-ZEPLIN (LZ)

TABLE II. Summary of DM relic density and direct detection constraints on the LSP neutralino.

The DD limits from the experimental collaborations are placed assuming that a single DM candidate constitutes the entire relic. Therefore, if the neutralino DM is underabundant, i.e., $\Omega_{\tilde{\chi}_1^0} < 0.118$, then the DD limits are applied on scaled cross-sections. The scaling factor ξ is taken unity when the LSP relic is within the experimental uncertainty, i.e., $0.118 < \Omega_{LSP} < 0.122$. For $\Omega_{LSP} < 0.118$, it is scaled by the ratio of the central value of the observed relic density to the computed relic density for $\tilde{\chi}_1^0$, as follows:

$$\xi = \frac{\Omega_{\tilde{\chi}_1^0}}{0.120} \quad (8)$$

The recent upper limit on the SI cross-section σ_{SI} derived by the LZ collaboration is roughly $\sim 3 - 4$ times stronger

than the previous most stringent limits from PandaX-4T in the region of DM masses considered in this work⁴. To demonstrate the role of the LZ result, we divide the constraints on our scanned parameter space into “**Before LZ**” which includes constraints from LEP, flavor, Higgs properties, heavy Higgs searches using `HiggsBounds`, relic density, and the DD experiments XENON-1T, PICO-60, and PandaX-4T, and “**After LZ**” with the constraint from the LZ experiment.

Although our scan is over a ten-dimensional parameter space, not all parameters contribute to the individual observables. The relic density is determined by the annihilation channels of the DM, which in the present scenario will dominantly proceed through the s -channel diagrams involving the Z and the Higgs bosons as propagators. Scattering between the neutralino and the SM quarks and gluons, which forms the basis of the DD experiments, will involve the same propagators in the t -channel. It is worth noting that diagrams involving squark exchange do not play an important role due to strong lower limits on squark masses from searches at the LHC. Therefore, the most important parameters for the DM constraints from relic density and the DD experiments are $-M_1$, M_2 , $|\mu|$, $\tan\beta$, and M_A , since these affect the couplings of the DM with the Z and Higgs bosons as shown in Eqns. 2 and 3. Large couplings are excluded by the DD experiments, whereas small values of couplings are excluded by the observed relic density constraint unless the mass of DM lies within a narrow window around half the mediator mass resulting in resonant enhancement of the DM annihilation cross-section.

In the Z funnel, the coupling depends only on the Higgsino components in the LSP, which decreases as we move to higher values of μ . Rewriting and simplifying Eqn. 3 for the lighter CP-even Higgs boson in the limit $M_A \gg M_Z$ (where $\cos\alpha \sim \sin\beta$), we have

$$g_{h\tilde{\chi}_1^0\tilde{\chi}_1^0} \approx -g(N_{12} - \tan\theta_W N_{11})(\sin\beta N_{14} - \cos\beta N_{13}) \quad (9)$$

Fig. 2 shows the coupling of the SM Higgs boson with the lightest neutralino as a function of the μ parameter (*top* panel) and $\tan\beta$ (*bottom* panel) for both positive (*left* panel) and negative (*right* panel) values of μ . For positive μ , the coupling is always negative and can increase in magnitude with decreasing value of μ and $\tan\beta$. For negative μ , the maximal value of the coupling increases for small $|\mu|$. Moreover, it can have either sign depending on the value of $\tan\beta$ – the coupling is negative at large $\tan\beta$ and it increases with decreasing $\tan\beta$, eventually becoming positive at low $\tan\beta$, around ~ 10 . Therefore, we can have large magnitude of coupling for both high and low values of $\tan\beta$.

The SI DD cross-section will further receive contribution from the heavy CP-even Higgs boson in the pMSSM (H) present in the t -channel, which has the following coupling to $\tilde{\chi}_1^0$ (from Eqn. 3):

$$g_{H\tilde{\chi}_1^0\tilde{\chi}_1^0} \approx g(N_{12} - \tan\theta_W N_{11})(\sin\beta N_{13} + \cos\beta N_{14}) \quad , \quad M_A \gg M_Z, \quad (10)$$

which has a sign opposite to the sign of μ . It couples to the SM up-type and down-type quarks as follows:

$$\begin{aligned} g_{Huu} &= i \frac{m_u}{v} \frac{\sin\alpha}{\sin\beta} \propto -\cot\beta \quad , \quad M_A \gg M_Z \\ g_{Hdd} &= i \frac{m_d}{v} \frac{\cos\alpha}{\cos\beta} \propto \tan\beta \quad , \quad M_A \gg M_Z \end{aligned} \quad (11)$$

The DM-quark scattering cross-section involves the product of the coupling $g_{H\tilde{\chi}_1^0\tilde{\chi}_1^0}$ with g_{Huu} or g_{Hdd} . For $\mu > 0$, the h and H contributions have opposite signs for up-type quarks, whereas for down-type quarks they add up, moreover, g_{Hdd} is $\tan\beta$ enhanced. The constructive interference between the contributions for down-type quarks is more effective than the destructive interference between the up-type quark contributions from h and H . For $\mu < 0$, when $\tan\beta$ is large and $g_{h\tilde{\chi}_1^0\tilde{\chi}_1^0}$ is negative, contributions from the two Higgs bosons destructively interfere for down-type quarks, and add up for up-type quarks. Since the cancellation is for coupling with down-type quarks, it is more effective for larger values of $\tan\beta$. For small $\tan\beta$, $g_{h\tilde{\chi}_1^0\tilde{\chi}_1^0}$ turns positive, and follows the same trend as for $\mu > 0$.

Having discussed the trends of the various couplings of the LSP DM, let us have a closer look at the Z and h funnels of both positive and negative μ and study how the recent LZ limit has affected these scenarios.

⁴ The LZ collaboration provides slightly stronger limits (~ 1.5 times better) than the recent XENON-nT experiment [60].

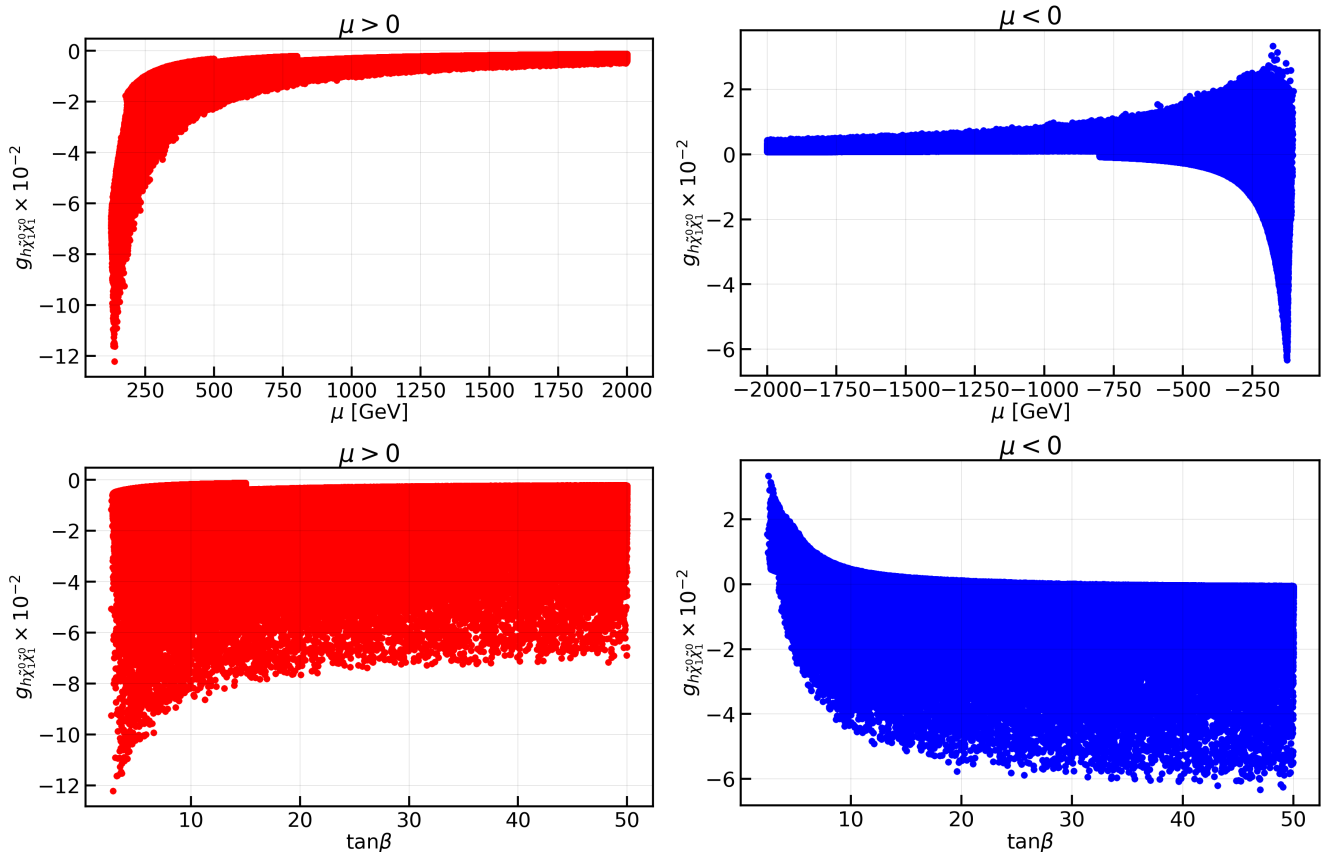


FIG. 2. Variation of the $g_{h\tilde{\chi}_1^0\tilde{\chi}_1^0}$ coupling with μ (top) and $\tan\beta$ (bottom) for $\mu > 0$ (left) and $\mu < 0$ (right) for points satisfying Higgs constraints, LEP and flavor constraints.

A. Z funnel

In the Z funnel, the observed relic density bound restricts $|\mu|$ to small values since the $g_{Z\tilde{\chi}_1^0\tilde{\chi}_1^0}$ coupling depends only on the Higgsino components of $\tilde{\chi}_1^0$. Fig. 3 shows the fraction of DM satisfied by the LSP, ξ , as a function of the NLSP neutralino mass ($M_{\tilde{\chi}_2^0}$) for both $\mu > 0$ and $\mu < 0$ with the “Before LZ” set of cuts. In both cases, beyond $M_{\tilde{\chi}_2^0} \sim 450$ GeV, DM becomes overabundant assuming the standard cosmological model.

For interpreting the constraints from the LZ experiment, we need to consider the $g_{h\tilde{\chi}_1^0\tilde{\chi}_1^0}$ coupling and the heavy Higgs contribution as well, which we discussed earlier. For $\mu > 0$, in the low $\tan\beta$ region, $g_{h\tilde{\chi}_1^0\tilde{\chi}_1^0}$ increases and in the high $\tan\beta$ region, the g_{Hdd} coupling gets enhanced, both increasing the SI DD cross-section. The scaled SI DD cross-section has two components – the SI DD cross section and the fraction of DM relic density produced by $\tilde{\chi}_1^0$. We plot the variation of these individual quantities as a function of the DM- h coupling in Fig. 4 top panel for the $\mu > 0$ scenario in the Z funnel. We divide the points in two regions of $\tan\beta$ – one from 5-20 (red) and another from 35-50 (blue). With decreasing magnitude of the coupling $g_{h\tilde{\chi}_1^0\tilde{\chi}_1^0}$, σ_{SI} decreases as expected. However, for the same value of the coupling, higher $\tan\beta$ values have slightly larger values of σ_{SI} , which is due to the $\tan\beta$ enhanced heavy Higgs contribution. For ξ , we observe the opposite trend with the coupling and $\tan\beta$.

Therefore, their product does not vary much, as shown in the left panel of Fig. 5 which displays the variation of $\sigma_{SI} \times \xi$ with $g_{h\tilde{\chi}_1^0\tilde{\chi}_1^0}$ for $\mu > 0$, with $\tan\beta$ in the colorbar. All of these points lie above the LZ bound and hence, all points are excluded. Since we require the product to be smaller than the LZ limit, we are interested in lower values of σ_{SI} and ξ . The lower edges in both the plots of Fig. 5 are not scattered and follow a trend. We also observe that we cannot achieve any lower value of ξ , and therefore, further populating the parameter space will not change our

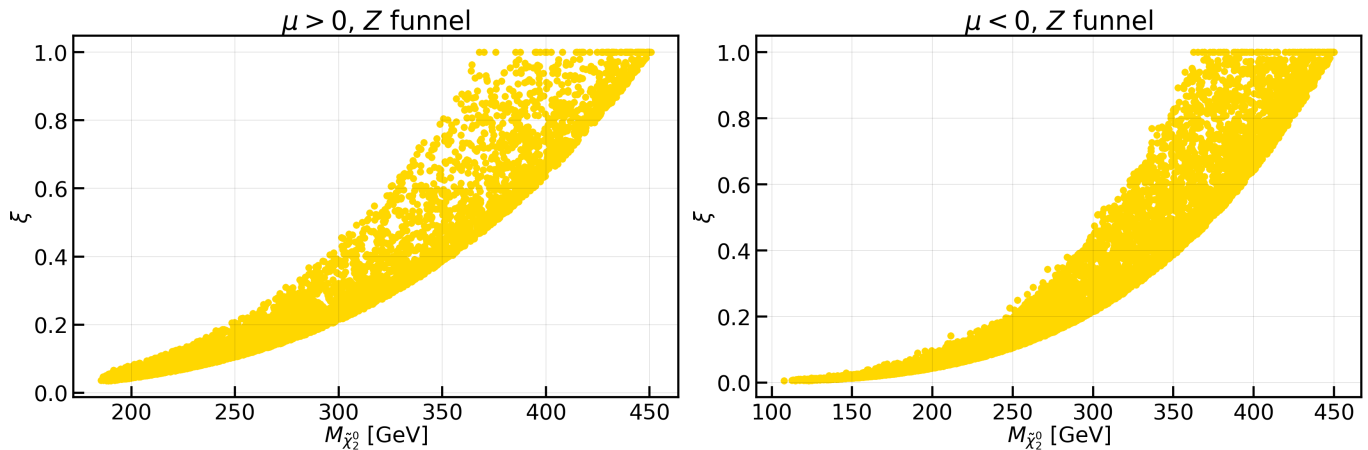


FIG. 3. Fraction of DM satisfied by $\tilde{\chi}_1^0$ ($\xi = \frac{\Omega_{\tilde{\chi}_1^0}^{\text{LSP}}}{0.120}$) as a function of $M_{\tilde{\chi}_2^0}$ for both $\mu > 0$ (left) and $\mu < 0$ (right) with the “Before LZ” set of cuts.

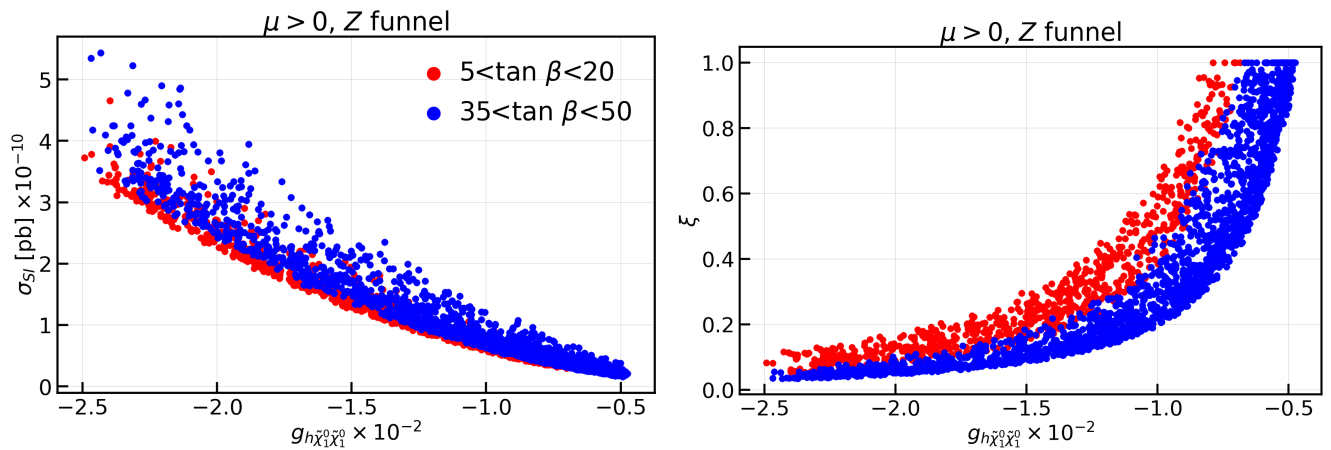


FIG. 4. Variation of σ_{SI} (top left) and ξ (top right) with the DM-light Higgs boson coupling for two different ranges of $\tan \beta$ for the $\mu > 0$ Z funnel.

conclusion regarding the exclusion of the Z funnel for the $\mu > 0$ scenario. This puts the Z funnel of $\mu > 0$ region under severe tension in the pMSSM, where we do not find any region of parameter space satisfying the relic density constraint and the LZ DD limit of $\sigma_{SI} \times \xi \lesssim 0.106 \times 10^{-10}$ pb, simultaneously.

The right panel of Fig. 5 shows a plot similar to the one in the left panel but for $\mu < 0$. For $\mu < 0$, we have seen that $g_{h\tilde{\chi}_1^0\tilde{\chi}_1^0}$ can attain very small values as it crosses zero coupling. Since we are in the Z funnel, the relic density is determined by $g_{Z\tilde{\chi}_1^0\tilde{\chi}_1^0}$ and smaller values of $|g_{h\tilde{\chi}_1^0\tilde{\chi}_1^0}|$ are allowed. These lead to very small $\sigma_{SI} \times \xi$, well below the present LZ limit. Moreover, for large $\tan \beta$, we have negative values of $g_{h\tilde{\chi}_1^0\tilde{\chi}_1^0}$ which leads to $\tan \beta$ enhanced cancellations from the heavy Higgs contribution. Therefore, the negative couplings have relatively smaller values of $\sigma_{SI} \times \xi$, as compared to the positive couplings, even when the magnitude of the coupling is the same. The entire region of parameter space with negative couplings, where there is an interference between the H and h contributions, satisfies the LZ limit. The future SDn DD experiments, which constrain the $g_{Z\tilde{\chi}_1^0\tilde{\chi}_1^0}$ coupling, play a much more crucial role in probing the parameter space in the Z funnel of $\mu < 0$, as we will later see in Fig. 13.

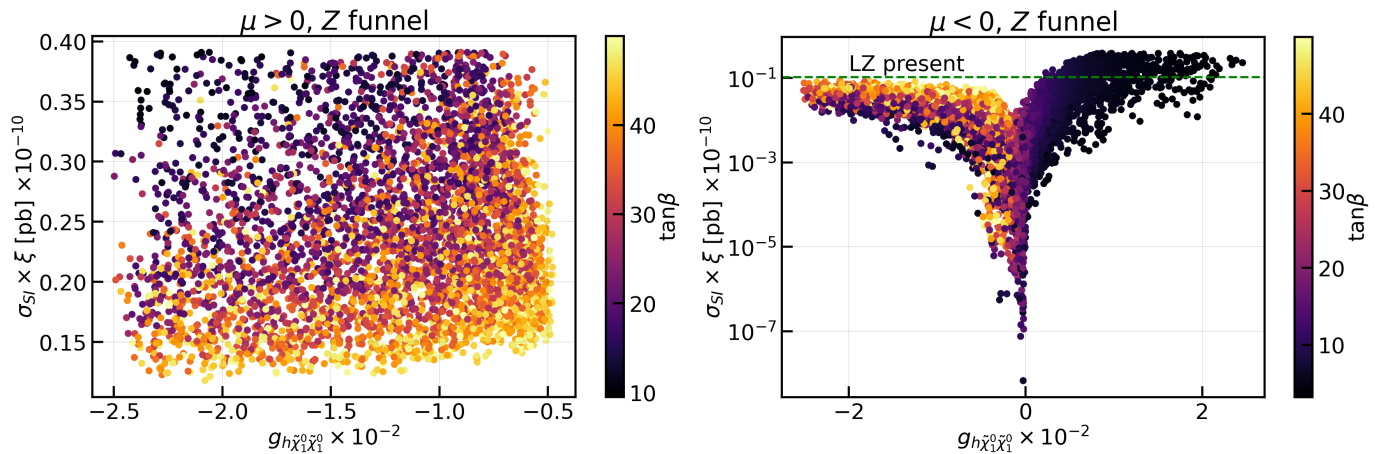


FIG. 5. Variation of the scaled SI DM-nucleon cross-section ($\sigma_{SI} \times \xi$) with $g_{h\tilde{\chi}_1^0\tilde{\chi}_1^0}$ for both $\mu > 0$ (left) and $\mu < 0$ (right) with the “Before LZ” set of cuts.

B. h funnel

As we move to the Higgs funnel, the LZ limit becomes slightly weaker than in the Z funnel. Moreover the relic density bound can be satisfied for Higgsinos heavier than ~ 450 GeV, unlike the Z funnel. This is because at high μ , the coupling $g_{h\tilde{\chi}_1^0\tilde{\chi}_1^0}$ can be large provided $\tan\beta$ is small (see Fig. 2).

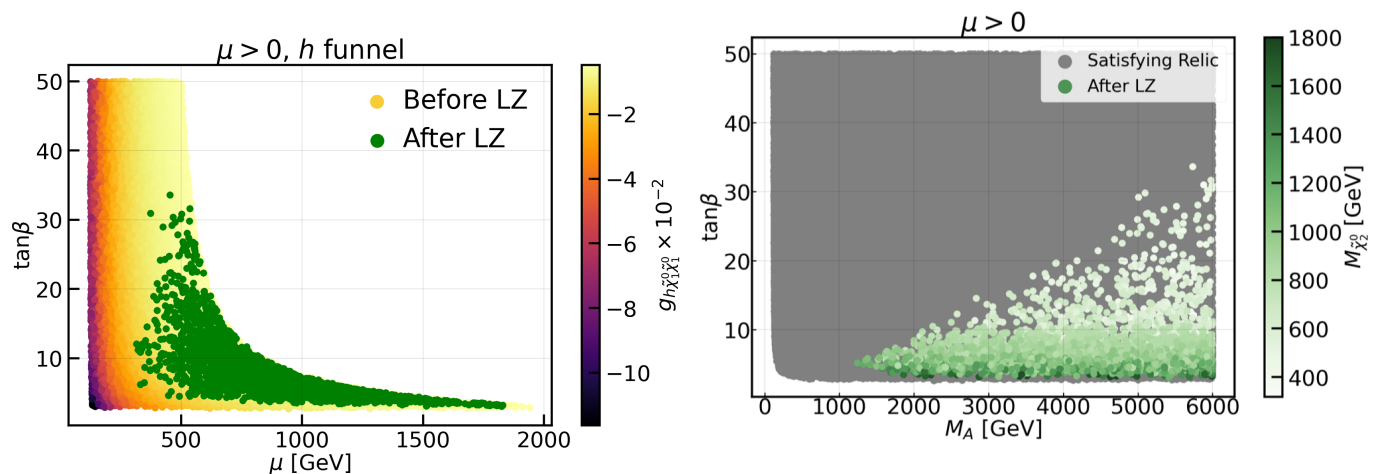


FIG. 6. Left: The $\mu > 0$ h funnel parameter space in the μ - $\tan\beta$ plane before (yellow) and after (green) applying the LZ limit [58] with $g_{h\tilde{\chi}_1^0\tilde{\chi}_1^0}$ in the colorbar for “Before LZ”. Right: The full $\mu > 0$ parameter space in the M_A - $\tan\beta$ plane that satisfy the relic density constraint (grey) and that satisfy all the constraints including LZ (green) with $M_{\tilde{\chi}_2^0}$ in the colorbar.

The left panel of Fig. 6 shows the parameter space points in the h funnel of $\mu > 0$ in the μ - $\tan\beta$ plane with the colorbar showing the value of $g_{h\tilde{\chi}_1^0\tilde{\chi}_1^0}$. The “Before LZ” set of constraints, especially the bound on relic density restricts large μ to have only small $\tan\beta$ values. The points shown in green in the left panel of Fig. 6 are allowed by the LZ limit. These points predominantly occupy regions characterised by smaller $g_{h\tilde{\chi}_1^0\tilde{\chi}_1^0}$, where μ is greater than around 400 GeV and $\tan\beta$ is smaller than 35⁵. Note that even though the points at higher values of $\tan\beta$ have very

⁵ These upper and lower bounds are provided just to give a qualitative idea, and might change with further scanning of points at the edge.

small couplings, they do not survive the LZ constraint due to the added $\tan\beta$ enhanced heavy Higgs contribution.

To further demonstrate the significant impact of the LZ result on the positive μ scenario, the *right* panel of Fig. 6 shows the $\mu > 0$ parameter space in the M_A - $\tan\beta$ plane satisfying the relic density constraint in *grey*. The parameter space obtained after imposing both the relic density and LZ bounds survives all the other set of cuts applied till this point, i.e., the constraints from Higgs properties, LEP, flavor and DD bounds on SDn and SDp cross-sections of the DM. These points are shown in shades of *green*. The *colorbar* in the *right* panel of Fig. 6 shows that the minimum allowed $M_{\tilde{\chi}_2^0}$ value is around 350 GeV. The LZ bound on SI DD constrains large $g_{h\tilde{\chi}_1^0\tilde{\chi}_1^0}$ values, ruling out lighter Higgsinos (see Fig. 2). Moreover, Higgsinos below 500 GeV are found at large values of $\tan\beta$ where the coupling $g_{h\tilde{\chi}_1^0\tilde{\chi}_1^0}$ is reduced and large M_A as can be seen in Fig. 6. Higher values of $\tan\beta$ are allowed as we go to large M_A where the heavy Higgs contribution decreases.

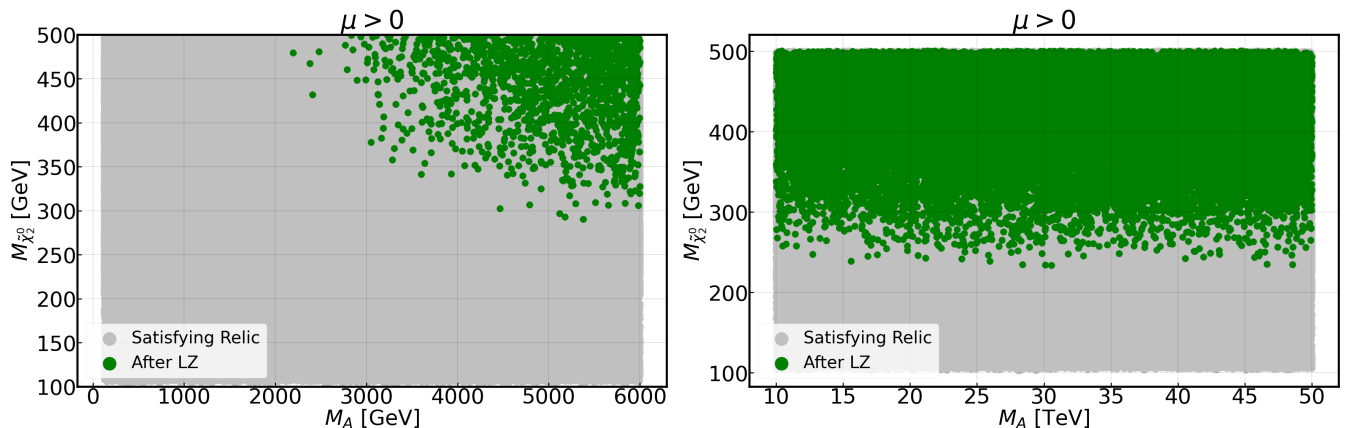


FIG. 7. Minimum allowed Higgsino mass after applying the DM constraints for a range of M_A between 100 GeV to 6 TeV (*left*) and 10 to 50 TeV (*right*). The points satisfying the relic density constraints are shown in *grey*, while the *green* colored points are allowed by the other current constraints including the LZ DD bound.

We have scanned M_A up to 6 TeV, and a natural question which arises is whether even larger M_A can decouple the effect of H and extend the allowed parameter space to include larger values of $\tan\beta$. This motivates us to perform a dedicated scan in the 10-50 TeV M_A region. Fig. 7 shows the parameter space in the $M_A - M_{\tilde{\chi}_2^0}$ plane for low M_A (*left*) and high M_A (*right*) regions. For low M_A (100 GeV - 6 TeV), the allowed points populate the upper right corner of the parameter space and the minimum value of $M_{\tilde{\chi}_2^0}$ decreases with increasing M_A . This trend is due to the heavy Higgs contribution which becomes smaller as we go to higher M_A values, and hence points with smaller values of $M_{\tilde{\chi}_2^0}$ survive the DM constraints. For our high M_A scan (10-50 TeV), the minimum value of $M_{\tilde{\chi}_2^0}$ is almost constant over the M_A range. However, higgsino masses below 200 GeV are still not allowed when we go to very high M_A values.

In the *left* panel of Fig. 8, we show the parameter points in the h funnel region of the $\mu < 0$ scenario in the $\mu - \tan\beta$ plane. The points are depicted under two conditions: firstly, all the constraints except the DD constraints are applied (*yellow*), and secondly, the most stringent SDn DD constraint from PandaX-4T is additionally applied (*green*). Note that the LZ limit is not applied on this parameter space yet. We observe that $\tan\beta$ is restricted to smaller values for large $|\mu|$, similar to the $\mu > 0$ scenario. The SDn DD cross-section depends on the coupling of the LSP with the Z boson, which grows with decreasing magnitude of μ , and therefore, the PandaX-4T SDn bound excludes low values of $|\mu|$. Regions of large $\tan\beta$ evade this bound, although $g_{Z\tilde{\chi}_1^0\tilde{\chi}_1^0}$ does not have any significant dependence on $\tan\beta$. The $\tan\beta$ dependence comes from the scaling factor ξ , since the $\tan\beta$ dependent $g_{h\tilde{\chi}_1^0\tilde{\chi}_1^0}$ coupling determines the relic density in the Higgs funnel.

We show values of ξ for the points passing the PandaX-4T SDn bound with $\tan\beta > 10$ as a function of $\tan\beta$ in

However, since these points lie very close to the LZ bound, the values of these bounds on μ and $\tan\beta$ won't be significantly affected.

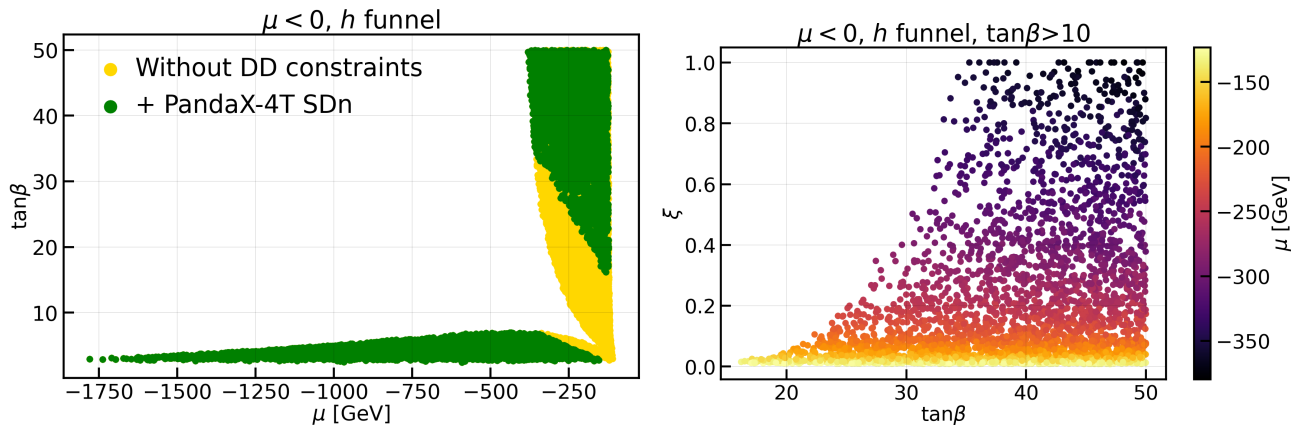


FIG. 8. *Left*: Parameter space points in the h funnel of $\mu < 0$ in the μ - $\tan\beta$ plane when all the constraints except the DD constraints are applied (in *yellow*), and in addition when the strongest available SDn DD constraint from the PandaX-4T experiment is applied (in *green*). *Right*: ξ values of the points passing the PandaX-4T SDn bound with $\tan\beta > 10$ as a function of $\tan\beta$ with the colorbar showing μ .

the *right* panel of Fig. 8 with the colorbar showing μ . The purpose of this is to show how points with low μ and high $\tan\beta$ survive the PandaX-4T bound on SDn cross-sections. It was shown in Fig. 2 that for $\mu < 0$, large magnitudes of $g_{h\tilde{\chi}_1^0\tilde{\chi}_1^0}$ are possible for large $\tan\beta$ and small μ . This makes ξ small and reduces the scaled SDn direct detection cross-section, even for low values of $|\mu|$, where otherwise the SDn cross-sections are high due to large $g_{Z\tilde{\chi}_1^0\tilde{\chi}_1^0}$ coupling. These high coupling values at high $\tan\beta$ also survive the SI DD bounds due to destructive contribution from the heavy Higgs boson. This region is particularly interesting since it involves light Higgsinos, which provide important benchmarks for Run-3 of LHC. For larger $|\mu|$, the $g_{h\tilde{\chi}_1^0\tilde{\chi}_1^0}$ coupling is smaller and larger $\tan\beta$ is required to increase ξ in order to satisfy the bound on SDn DD cross-section.

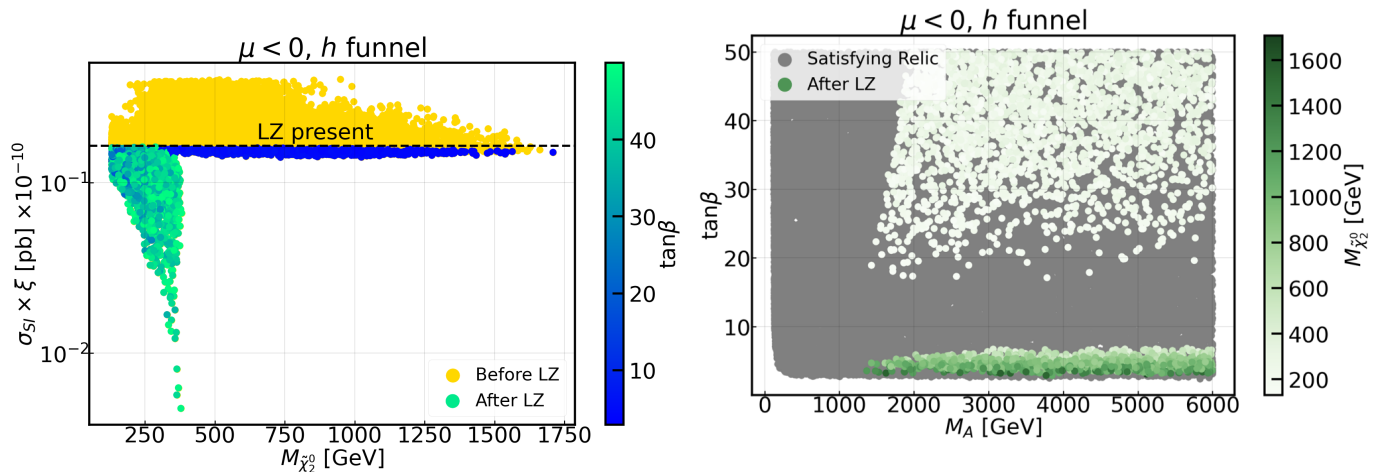


FIG. 9. *Left*: The h funnel of the $\mu < 0$ in the $M_{\tilde{\chi}_2^0}$ - $\sigma_{SI} \times \xi$ plane before and after the LZ limit. *Right*: The h funnel of the $\mu < 0$ in the M_A - $\tan\beta$ plane satisfying various cuts, and allowed points with $M_{\tilde{\chi}_2^0}$ in the *colorbar*.

To understand the effect of the LZ result, the *left* panel of Fig. 9 shows the parameter space in the $M_{\tilde{\chi}_2^0}$ - $\sigma_{SI} \times \xi$ plane for the h funnel for $\mu < 0$ before and after the LZ result. This includes the SDn constraint from PandaX-4T, which we discussed in Fig. 8. The *colorbar* in the plot indicates the corresponding $\tan\beta$ values. LZ excludes a significant part of the parameter space, especially for high μ values corresponding to large $M_{\tilde{\chi}_2^0}$, where only a narrow strip of allowed

region with very small $\tan\beta$ remains. With only a 20% improvement in the LZ limit in the future, this region can be fully probed. The very low SI DD cross-sections found for Higgsinos in the mass range 200-400 GeV is due to the destructive interference between the h and H contributions which is more important at large $\tan\beta$. The *right* panel of the same figure shows the allowed parameter space in the M_A - $\tan\beta$ plane, with $M_{\tilde{\chi}_2^0}$ in the *colorbar*. The gap in the allowed region around $\tan\beta$ values of 6-18 is due to the recent bound on SDn cross-section by the PandaX-4T collaboration, as we observed previously in Fig. 8.

The upshot for $\mu > 0$ scenario is that after the DM constraints, the Z -funnel is excluded by the LZ result, however, a region of the h -funnel survives these constraints. In this region, the lightest allowed Higgsino is around 350 GeV. For the $\mu < 0$ scenario, we found allowed points both in the Z and h funnel, and Higgsinos as light as 125 GeV survive DM constraints. The major factor that creates a difference between the results of positive and negative μ is the effect of the heavy Higgs bosons in the DD cross-sections.

C. Comparison with a simplified model

The previous section has shown the importance of the heavy Higgs boson contribution to the SI DD cross-section and its dependence on $\tan\beta$ in pMSSM. As we move towards heavier Higgsinos, the relic density upper bound can only be satisfied at very low values of $\tan\beta$ for both $\mu > 0$ and $\mu < 0$. In this region, the effect of H is decoupled, and the lighter Higgs boson plays the dominant role. It is worth studying whether our results for high μ in pMSSM with the DM constraints, especially the interplay of relic density and the recent LZ upper limit on the SI DD cross-section, generalise to any BSM theory consisting of a Majorana fermion coupling with only the light Higgs boson, which resembles the discovered Higgs boson at LHC.

We consider a simplified model where the SM is extended by a single Majorana fermion, χ , which is the DM candidate. It has coupling with the SM Higgs boson ($g_{\chi h}$) and has the following Lagrangian:

$$\mathcal{L} = \mathcal{L}_{SM} + g_{\chi h} \chi \bar{C} \chi h. \quad (12)$$

We scan over the mass of the DM and its coupling with h , i.e., in the $M_\chi - g_{\chi h}$ plane. The Higgs boson mass is fixed at 125 GeV, and the total width of h is calculated from the model. Since this minimal model has only two input parameters, M_χ and $g_{\chi h}$, the total width of the Higgs boson has negligible variation and attains a value around 4.02 MeV when the model is implemented in MicrOMEGAS 5.2.13.

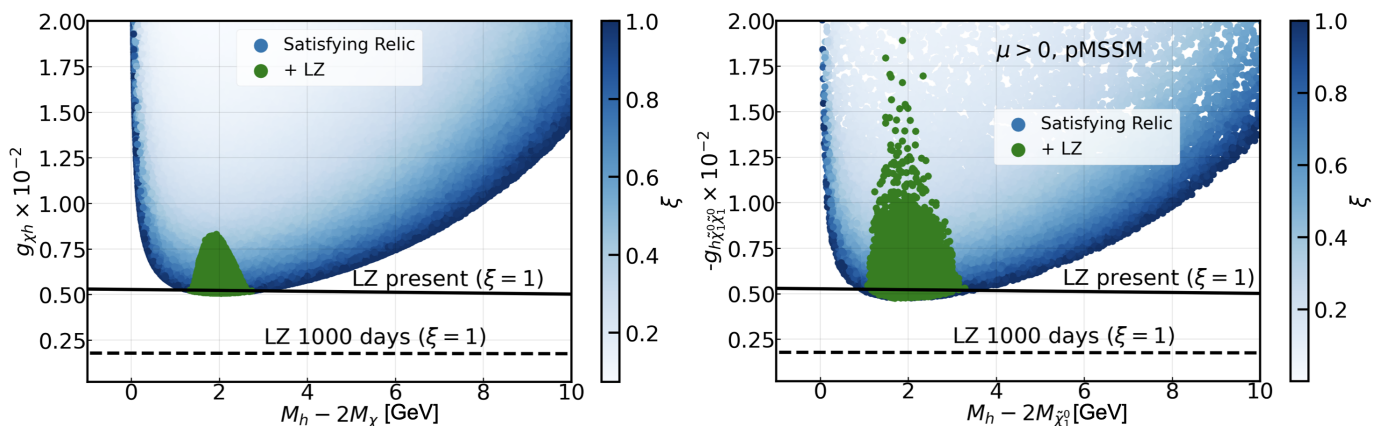


FIG. 10. Result from the scan of a simplified model where we extend the SM by a Majorana fermion coupled to the h boson (*left*) and the $\mu > 0$ scenario of pMSSM (*right*) in the $g_{\chi h} - (M_h - 2 \times M_\chi)$ plane. The *blue* points satisfy the relic density upper bound with ξ shown in the colorbar, and the *green* points also satisfy the LZ limit.

The DM relic density depends on the couplings involved in the annihilation process, the difference between twice the DM mass and the resonance in the funnel region, and the width of the mediator particle. The coupling of the Higgs boson to the SM particles and the width of the Higgs boson do not vary much in this set-up, the only variables are therefore $M_h - 2M_\chi$ and $g_{\chi h}$. The contribution of DM to the total width of h is negligible. Moreover, the scattering cross-section of $\tilde{\chi}$ on nucleons relevant for DD depends on the same coupling. We present our results of the scan in the plane of $M_h - 2M_\chi$ versus $g_{\chi h}$. The *left* panel of Fig. 10 shows the region of parameter space surviving the relic density constraint in *blue* with the *colorbar* showing the fraction of DM constituted by this additional fermion, and the allowed region of parameter space after the LZ DD bound in *green*. We find that the coupling allowed by both relic density and DD is minimum when $M_h - 2M_\chi \sim 2$ GeV. Furthermore, $g_{\chi h}$ cannot be much smaller than ~ 0.005 in order to satisfy these two constraints. The region of parameter space that satisfies current constraint can be probed by improving the DD limit by $\sim 11\%$, which should be achieved in a few days of running of LZ.

The result for the simplified scenario makes it clear that the relic density and the recent LZ limit strongly constrain the coupling and mass plane of the DM when it connects to the SM particles through a Higgs portal. Therefore, even in a BSM theory like pMSSM, where we have a wide range of input parameters, the parameter space is equally constrained. The *right* panel of Fig. 10 shows an analogous plot for the $\mu > 0$ scenario of pMSSM for heavier Higgsinos ($\mu \gtrsim 850$ GeV). For $\mu < 0$ scenario of pMSSM where $|\mu|$ is kept higher than ~ 850 GeV, we get a similar result. The key difference that we observe in the pMSSM for large $|\mu|$ is that few points with larger coupling ($g_{\chi h} \sim 0.01 - 0.025$) are still allowed by the LZ limit, unlike the simplified scenario. This is partly due to the larger variation of the Higgs boson mass in the pMSSM scan, while in the simplified model, it is fixed to 125 GeV. Indeed a tighter constraint on the Higgs boson mass in the pMSSM affects slightly the range of allowed values for both the coupling and the mass difference $M_h - 2M_{\tilde{\chi}_1^0}$ as will be discussed in Fig. 12. Moreover, even for the same Higgs boson mass, coupling and DM mass, the total width of the Higgs boson in the pMSSM is different than in the simplified model due to the higher order corrections in $\Gamma(h \rightarrow b\bar{b})$ coming from Δm_b corrections [102–105]. Therefore, some of the points with larger couplings marginally pass the LZ limit in the pMSSM because the smaller width implies a lower value for the relic density, thereby reducing ξ . However, the constraints from the Higgs signal strength measurements do not allow Γ_h to deviate significantly from the SM prediction, which limits its effect on our results.

V. ELECTROWEAKINO CONSTRAINTS AND THE ALLOWED PARAMETER SPACE

The electroweakinos can be directly produced at the colliders, where the NLSP Higgsinos ($\tilde{\chi}_1^\pm/\tilde{\chi}_2^0/\tilde{\chi}_3^0$) can decay to final states involving the LSP neutralino ($\tilde{\chi}_1^0$) along with W , Z or h bosons, which can have both leptonic and hadronic decays. We use the `SModelS 2.2.1` [106–113] package to implement the electroweakino search constraints on our scanned parameter space. Recently many analyses have updated their results with the full Run-2 data and this version of `SModelS` includes results from the recent search for electroweakinos in the leptonic final states at CMS [49] and ATLAS [50] and in the hadronic final states at ATLAS [51]. The constraints from the recent searches play a significant role in excluding a large range of $M_{\tilde{\chi}_1^\pm}$, $M_{\tilde{\chi}_2^0}$ and $M_{\tilde{\chi}_3^0}$, extending the sensitivity to higher masses, especially with the ATLAS analysis of the hadronic final states.

We apply the limits from electroweakino searches on the parameter space surviving all the constraints discussed previously in Sections 3 and 4, which are defined as “**After LZ**”. We identify regions of the parameter space surviving all the constraints: A) high values of $|\mu|$ ($\gtrsim 800$ GeV) with low $\tan\beta$ ($\lesssim 10$) in the h funnel of both positive and negative μ , and B) low values of $|\mu|$ ($\lesssim 200$ GeV) in both the Z and h funnels of negative μ . We perform dedicated scans over these regions again with an additional sample of size $\sim 10^8$, which makes the total number of points scanned for our analysis to be $\sim 3 \times 10^8$. From these 3×10^8 points, around 41% pass the Higgs boson mass condition. This is due to the fact that we perform our scans with very high values of $M_{\tilde{Q}_{3L}}$, $M_{\tilde{t}_R}$, and $M_{\tilde{b}_R}$, starting from 3 TeV and vary A_t from -20 TeV to 20 TeV, which helps in satisfying the Higgs mass condition.

Let us first discuss the results in the positive μ scenario. Fig. 11 (*left* panel) shows the scaled SI DM-nucleon

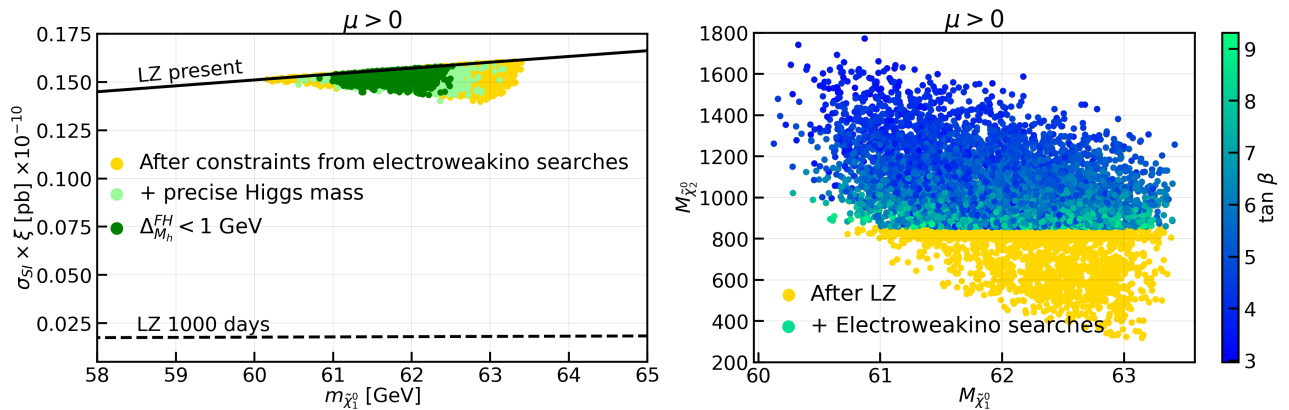


FIG. 11. *Left*: Scaled SI DM-nucleon cross-section ($\sigma_{SI} \times \xi$) for $\mu > 0$ as a function of the mass of the LSP neutralino DM in the region of parameter space satisfying LEP, flavor, Higgs constraints, relic density, DM DD constraints from the XENON-1T, PICO-60, PandaX-4T, and LZ experiments, the electroweakino limits implemented in `SModelS`, and the precise Higgs mass condition with $\Delta_{M_h}^{FH} < 1$ GeV; *Right*: Parameter space satisfying all the constraints defined as “**After LZ**” and the region surviving the electroweakino searches in the $M_{\tilde{\chi}_1^0} - M_{\tilde{\chi}_2^0}$ plane for $\mu > 0$, where the *colorbar* shows $\tan \beta$.

cross-section ($\sigma_{SI} \times \xi$) with the mass of the LSP neutralino DM for the allowed parameter space for $\mu > 0$. In the *right* panel of Fig. 11, we show these points in the $M_{\tilde{\chi}_1^0} - M_{\tilde{\chi}_2^0}$ plane with $\tan \beta$ in the *colorbar*. In Section IV, we have discussed that the LZ limit excludes the Z funnel region for $\mu > 0$. As a result, both the panels of Fig. 11 have allowed points only in the h funnel region.

The *right* panel of Fig. 11 reveals that on applying the electroweakino constraints implemented in `SModelS`, $M_{\tilde{\chi}_2^0} \lesssim 850$ GeV are excluded by various collider searches. The allowed region of higgsinos heavier than 850 GeV populates very small values of $\tan \beta$, which results from the DM constraints as we have discussed earlier in Section IV B. The region of parameter space surviving the constraints from electroweakino searches can be probed by improving the LZ limit by 20% which can be achieved with just a few more days of running, as can be seen from the *left* panel of Fig. 11. For the simplified scenario, note that only 11% improvement in the LZ bound is required to probe the allowed parameter region, which is smaller than that required for the pMSSM parameter space. The difference in the two scenarios is again due to the variation in the Higgs boson total decay width. The coupling $g_{h\tilde{\chi}_1^0\tilde{\chi}_1^0}$ for heavier Higgsinos becomes constant, and since the surviving regions are restricted to low $\tan \beta$ values, there is no significant contribution from the heavy Higgs. This parameter space cannot have any smaller values of $\sigma_{SI} \times \xi$, as the relic density constraint does not allow for lower values of the coupling.

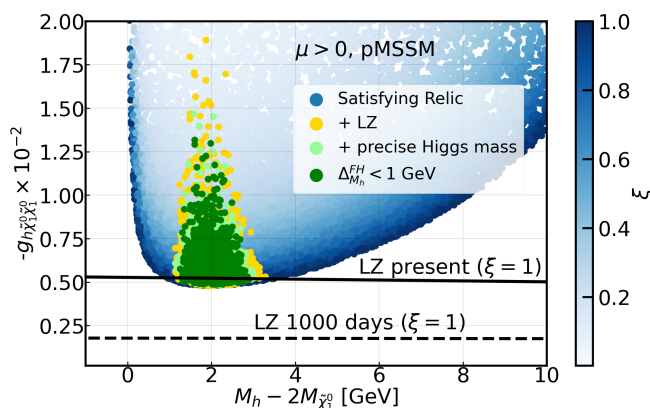


FIG. 12. The allowed regions for the $\mu > 0$ scenario of pMSSM in the $g_{\chi h} - (M_h - 2 \times M_{\tilde{\chi}_1^0})$ plane to show the impact of the precise Higgs mass condition.

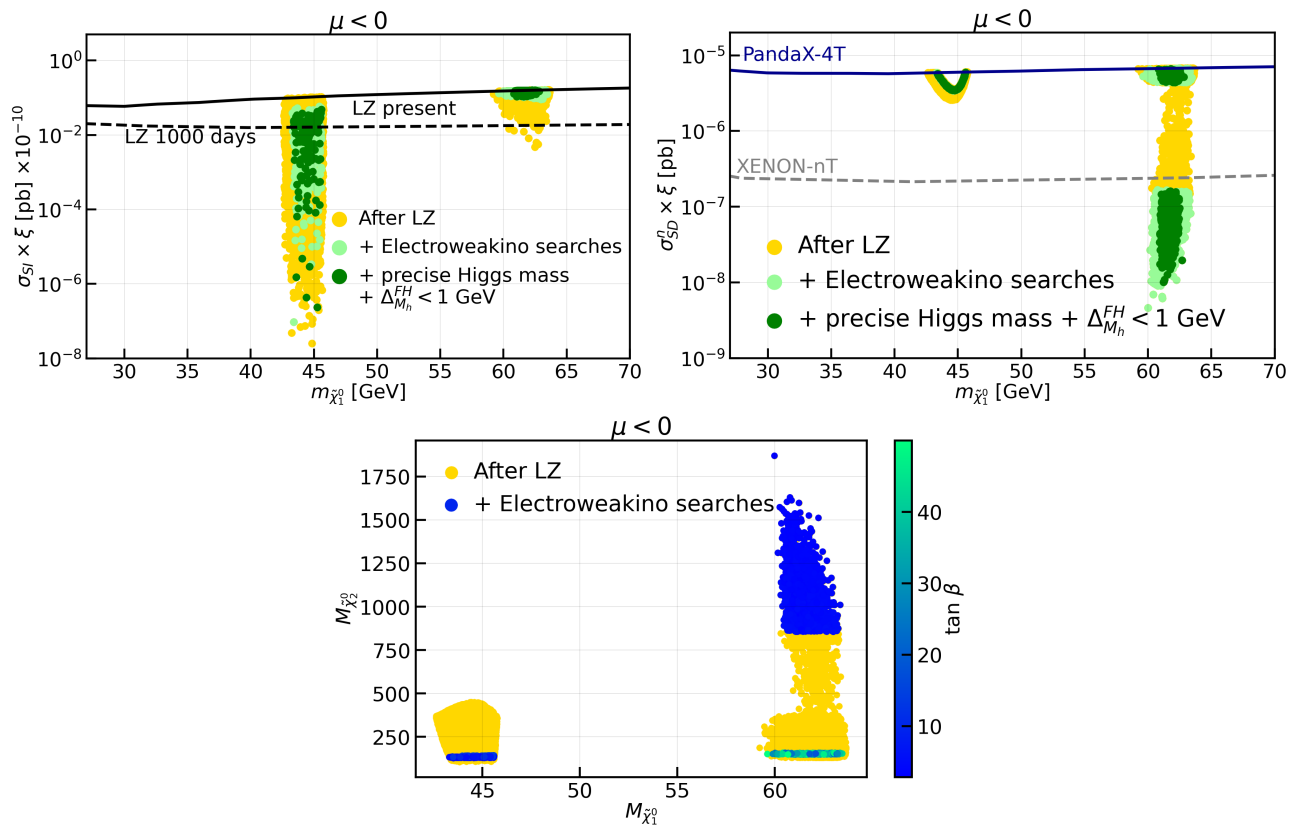


FIG. 13. *Top*: Scaled SI DM-nucleon cross-section ($\sigma_{SI} \times \xi$, *left*) and scaled SD DM-neutron cross-section ($\sigma_{SDn} \times \xi$, *right*) for $\mu < 0$ as a function of the mass of the LSP neutralino DM in the region of parameter space satisfying LEP, flavor, Higgs constraints, relic density, and DM DD constraints from the XENON-1T, PICO-60, PandaX-4T, and LZ experiments (shown in *yellow* and marked “**After LZ**”), after applying the electroweakino limits implemented in `SModelS`, and after the precise Higgs mass condition with $\Delta_{M_h}^{FH} < 1$ GeV; *Bottom*: Parameter space satisfying all the constraints defined as “**After LZ**” and the regions surviving the electroweakino searches in the $M_{\tilde{\chi}_1^0}$ - $M_{\tilde{\chi}_2^0}$ plane for $\mu < 0$, where the *colorbar* shows $\tan \beta$.

Although the Higgs mass can have large theoretical uncertainties, the experimentally measured value of the Higgs mass has a very small error bar. This impacts the allowed mass range of the neutralino, since the relic density is very sensitive to the mass difference between the neutralino from the Higgs funnel. In Fig 11 the dark green points illustrate the impact of imposing the precise Higgs mass condition with $\Delta_{M_h}^{FH} < 1$ GeV on the allowed range of the neutralino DM mass. Similar results on the range of allowed neutralino masses are obtained when performing a dedicated scan where we impose that the uncertainty on the Higgs mass predicted from `FeynHiggs` is below 1 GeV and $M_h \pm \Delta_{M_h}^{FH} \in [125.38 - 2 \times 0.14 \text{ GeV}, 125.38 + 2 \times 0.14 \text{ GeV}]$, i.e., within 2σ of the experimentally measured mass of the Higgs boson. In Fig. 12, we show the impact of restricting the Higgs mass close to the experimentally measured value on the coupling- $M_h - 2M_{\tilde{\chi}_1^0}$ plane. Moreover, we find that the allowed points mostly concentrate near $M_h - 2M_{\tilde{\chi}_1^0} \sim 1 - 3$ GeV, irrespective of the 3 GeV Higgs mass window or the more precise Higgs mass condition from `FeynHiggs`. In the next section, we choose our benchmark points from this region where the theoretically estimated Higgs mass is not far from the experimental value.

For the negative μ scenario, the *top* panels of Fig. 13 show the scaled SI DM-nucleon cross-section ($\sigma_{SI} \times \xi$, *left*) and scaled SD DM-neutron cross-section ($\sigma_{SDn} \times \xi$, *right*) as a function of the mass of the LSP neutralino DM. We observe that we have regions of parameter space which survive all the constraints in both the Z and the h funnels. The *top left* panel of Fig. 13 shows that the allowed region in the h funnel is well within the reach of the next few days of LZ data which can improve the limit on SI DD cross-section by 80%, and from the *top right* panel, we infer that the allowed parameter space in the Z funnel can be probed by the SDn result projected by the XENON-nT collaboration.

The *bottom* panel of Fig. 13 shows the parameter space in the $M_{\tilde{\chi}_1^0}$ - $M_{\tilde{\chi}_2^0}$ plane for $\mu < 0$, with the *colorbar* representing $\tan\beta$, for the points allowed by all the constraints. The electroweakino searches restrict the allowed parameter space to either heavy Higgsinos, having masses $\gtrsim 850$ GeV, or to a narrow region of parameter space with light Higgsinos with masses in the range of 125-145 GeV in the Z -funnel and 145-160 GeV in the h -funnel, many of which have very small R -values⁶. We further investigate the allowed region of such light Higgsinos in the following section. Fig. 11 and Fig. 13 are similar to Figs. 1 and 2 of Ref. [47], they are shown here for completeness. We also show the impact of using a tighter constraint on the Higgs mass in Figs. 11 and 13. The *right* panel of Fig. 11 and the *bottom* panel of Fig. 13 also show the $\tan\beta$ range of the allowed regions in the *colorbar*.

The future lepton colliders like ILC and CEPC will be crucial for precision measurements of Higgs boson. The projected upper limit on the invisible branching of the Higgs boson is 0.4% at ILC [114] and 0.3% at CEPC [115]. Although these can probe a significant part of the allowed parameter space in the $\mu < 0$ case, as shown in Fig. 23 in Appendix A, we still have regions with $\text{Br}(h \rightarrow \text{invisible}) < 0.003$ in both the Z and h -funnels. In the $\mu < 0$ case, the partial decay width of the Z boson to $\tilde{\chi}_1^0$ ($\Gamma_{\text{inv}}^{\text{new}}$) is always less than 0.1 MeV for the allowed parameter region that we obtain. Therefore, we do not expect the Giga- Z option of ILC, which is expected to have a modest improvement over LEP [116], to be sensitive to this region.

The relic density can have theoretical uncertainties in its calculation [117–119]. If we overestimate the relic density by few percent as compared to its actual value due to the theoretical uncertainties, the scaling factor, ξ , reduces, resulting in a lower SI DD cross-section. Fig. 14 shows the scaled SI DD cross-section ($\sigma_{SI} \times \xi$) with the DM mass of the parameter space for $\mu > 0$ surviving the “**After LZ**” set of constraints assuming that the relic density is overestimated by 20%, with the *colorbar* showing the mass of $\tilde{\chi}_2^0$. We observe that a small allowed region has opened up in the Z funnel which survives the present LZ result. However, the Higgsinos have masses above ~ 200 GeV, and get excluded by the collider bounds from electroweakino searches, as we have seen from the *bottom* panel of Fig. 13. In the h funnel, the allowed region extends further down to $\sigma_{SI} \times \xi \sim 0.112 \times 10^{-10}$ pb as compared to our result with no theoretical uncertainty on the relic density, where the allowed region in the h funnel had the lowest scaled SI DD cross-section of around 0.137×10^{-10} pb. Still, this region is well within the projected limit from the full 1000 days of the LZ experiment.

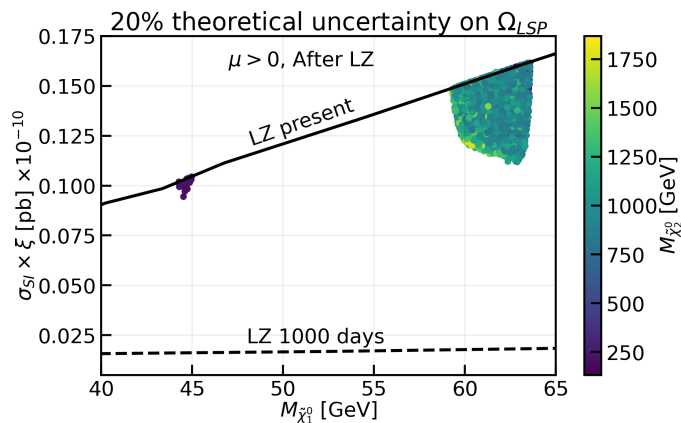


FIG. 14. Scaled SI DM-nucleon cross-section ($\sigma_{SI} \times \xi$) for $\mu > 0$, with 20% overestimation of relic density due to theoretical uncertainty, as a function of the mass of the LSP neutralino DM in the region of parameter space satisfying LEP, flavor, Higgs constraints, relic density, and DM DD constraints from the XENON-1T, PICO-60, PandaX-4T, and LZ experiments, defined as “**After LZ**”.

Let us now focus on the regions of light Higgsinos allowed by the present electroweakino searches.

⁶ R -value is the ratio of the signal cross-section and the experimentally allowed upper bound on the cross-section of a BSM process in a particular final state. A smaller R -value indicates that the parameter space point is allowed and lies way outside the current limit, whereas a R -value greater than 1 indicates that the signal is excluded.

VI. COLLIDER ANALYSES FOR PROBING THE LIGHT HIGGSINOS

In this section, we study the surviving regions of parameter space with lighter Higgsinos in the standard cosmological scenario. In Fig. 15, taken from Ref. [47], we present the R -value as given by the **SModelS** package for the most sensitive analyses on the allowed parameter space in the Z (left) and h funnel (right) of the negative μ scenario. This includes ATLAS analyses for the final states 2 leptons (e, μ) + MET and 3 leptons (e, μ, τ) + MET with 20.3 fb^{-1} of data, along with final states having jets + MET and 3 leptons + MET with an integrated luminosity of 139 fb^{-1} . The relevant CMS analyses include searches for electroweakinos with decays to leptons, W , Z , and Higgs bosons with a luminosity of 19.5 fb^{-1} and multilepton final states with 35.9 fb^{-1} . We observe that many of these points have very low R -values which indicate low sensitivity of the collider searches. The sensitivity drops around the region where the mass difference between the $\tilde{\chi}_1^\pm/\tilde{\chi}_2^0$ and the $\tilde{\chi}_1^0$ is close to the mass of the Z boson. Since in this region the decay products of the NLSP electroweakinos are produced at rest, the $\tilde{\chi}_1^0$ does not carry significant momentum, thereby, decreasing the effectiveness of the p_T^{miss} variable to differentiate the signal from SM backgrounds. Therefore, the experimental results suffer from low sensitivity near the Z boson mass threshold.

Representative benchmarks from each of the allowed regions of the parameter space are presented in Table III. These benchmarks have very small uncertainty in the Higgs boson mass as estimated by **FeynHiggs** ($\Delta_{M_h}^{FH} \lesssim \mathcal{O}(1) \text{ GeV}$), and have **SModelS** R -values below 0.5⁷. They are also allowed when tested with **CheckMATE 2** [121], another package that implements the constraints from electroweakino searches. We find that the Tevatron searches for light charginos [122] are also not sensitive to these benchmarks.

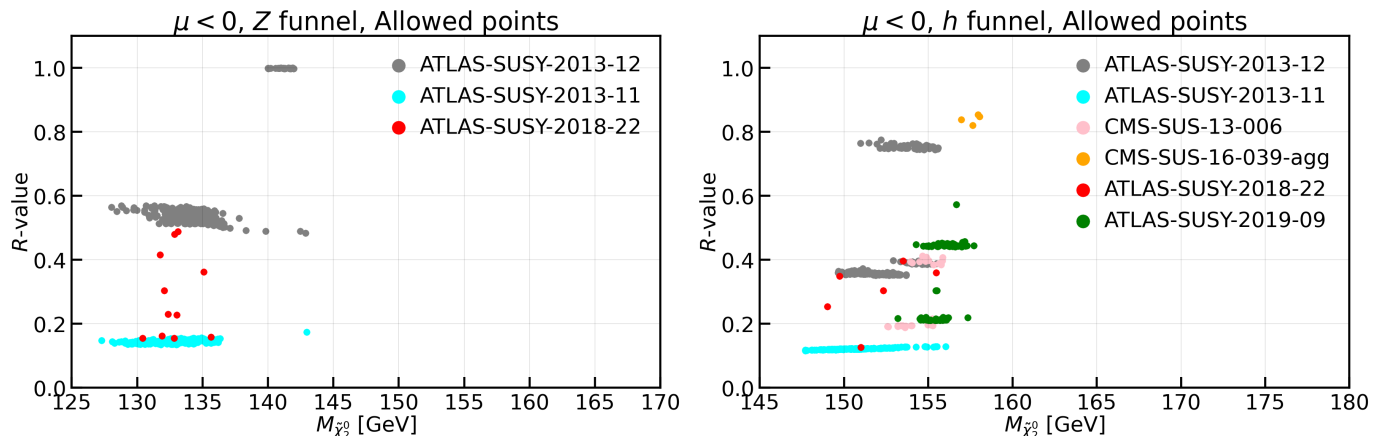


FIG. 15. R -values from **SModelS-2.2.1** of the most sensitive analyses versus the $M_{\tilde{\chi}_2^0}$ for the light Higgsino scenarios allowed for $\mu < 0$ in the Z funnel (left) and h funnel (right). The different colors depict the most sensitive analysis for each point.

⁷ These benchmarks survive the electroweakino searches implemented in the latest version of **SModelS-2.3.0** [120]. We discuss the impact of combination of analyses implemented in **SModelS-2.3** on our benchmark points in Appendix C.

Benchmarks (<i>mass parameters in GeV</i>)			$M_h[\Delta_{M_h}^{FH}]$ [GeV]	$\sigma_{SI} \times \xi \times 10^{-10}$ [pb]	
$\mu > 0$	<i>h</i> -funnel	BP1	$M_t = 173.21, M_1 = 62.5, M_2 = 2000, \mu = 1000, \tan\beta = 5, M_A = 3000,$ $M_{\tilde{Q}_{3L}} = 10000, M_{\tilde{t}_R} = 10000, M_{\tilde{b}_R} = 10000, A_t = 10000, M_3 = 3000$	125.38 [±0.97]	0.151
$\mu < 0$	<i>Z</i> -funnel	BP2	$M_t = 173.21, M_1 = 44, M_2 = 2000, \mu = -124, \tan\beta = 5, M_A = 3000,$ $M_{\tilde{Q}_{3L}} = 10000, M_{\tilde{t}_R} = 10000, M_{\tilde{b}_R} = 10000, A_t = 10000, M_3 = 3000$	125.88 [±0.96]	7.46×10^{-4}
	<i>h</i> -funnel	BP3	$M_t = 173.21, M_1 = 68, M_2 = 2000, \mu = -150, \tan\beta = 50, M_A = 3000,$ $M_{\tilde{Q}_{3L}} = 5000, M_{\tilde{t}_R} = 5000, M_{\tilde{b}_R} = 5000, A_t = -5000, M_3 = 3000$	125.67 [±0.63]	0.143
		BP4	$M_t = 173.21, M_1 = 61, M_2 = 2000, \mu = -1000, \tan\beta = 4.5, M_A = 3000,$ $M_{\tilde{Q}_{3L}} = 10000, M_{\tilde{t}_R} = 10000, M_{\tilde{b}_R} = 10000, A_t = 10000, M_3 = 3000$	125.15 [±0.99]	0.150

TABLE III. Parameters corresponding to four benchmark points satisfying all the present constraints from the $\mu > 0$ and $\mu < 0$ scenarios along with their scaled SI DD cross-sections. The mass of the Higgs boson M_h and the uncertainty in M_h computed by FeynHiggs ($\Delta_{M_h}^{FH}$) are also shown.

For probing the benchmarks with heavy Higgsinos, BP1 and BP4, the hadronic decay channels of the W and Z bosons are more sensitive than the leptonic ones. The current ATLAS result for the hadronic final state excludes Higgsinos below 850 GeV (*right* panel of Fig. 11). Assuming that the upper limit on the cross-section improves by a factor of $\sqrt{\mathcal{L}}$ with increasing luminosity, \mathcal{L} , Run-3 will be able to probe Higgsinos up to a mass of 900-925 GeV and HL-LHC will further increase the sensitivity to ~ 1100 GeV. Therefore, BP1 and BP4 can be interesting benchmarks to be probed in the HL-LHC runs.

Our benchmarks for light Higgsinos survive the electroweakino constraints as implemented in recasting frameworks like `SModelS` and `CheckMATE`. However, it is not guaranteed that all the recent relevant public results from the experimental collaborations have been added in the database of these packages. This motivates a detailed analysis for such light Higgsinos, which we present in the subsequent section.

To estimate the prospects for probing the region with light charginos and neutralinos at the LHC, we perform an analysis of the low mass Higgsino-like electroweakinos in the leptonic $3l + \cancel{E}_T$ final state at $\sqrt{s} = 14$ TeV using the `XGBOOST` [123] framework. We study the process $pp \rightarrow \tilde{\chi}_1^\pm \tilde{\chi}_2^0 / \tilde{\chi}_1^\pm \tilde{\chi}_3^0, \tilde{\chi}_1^\pm \rightarrow f f' \tilde{\chi}_1^0, \tilde{\chi}_2^0 / \tilde{\chi}_3^0 \rightarrow f \tilde{f} \tilde{\chi}_1^0$ with $M_{\tilde{\chi}_1^\pm} = 125.1$ GeV, $M_{\tilde{\chi}_2^0} = 129.9$ GeV, $M_{\tilde{\chi}_3^0} = 133.5$ GeV, and $M_{\tilde{\chi}_1^0} = 44.6$ GeV (BP2 from Table III) where f, f' are SM fermions. We restrict to the leptonic final state which is cleaner for a lighter benchmark, such as ours. The SM background processes studied in the analyses are summarised in Table IV with their respective cross-sections and simulation details.

Background	Cross section [pb]	Generated using	Total generated
$ll\nu$	0.4684×1.2	MadGraph 2.7.3	9.98×10^6
WZ , leptonic, $2j$ matched	1.253×1.2	MadGraph 2.7.3	4.97×10^6
ZZ , leptonic, $2j$ matched	0.1186×1.2	MadGraph 2.7.3	1.25×10^6
$t\bar{t}$, leptonic	55.36×1.74	MadGraph 2.7.3	6×10^7
VVV , inclusive	0.2678×1.2	MadGraph 2.7.3	2.5×10^6
Wh , inclusive	1.504 [124]	Pythia 8.306	5×10^6
Zh , inclusive	0.883 [124]	Pythia 8.306	5×10^6
ggF $h \rightarrow ZZ$, leptonic	0.0137	Pythia 8.306	5×10^6
VBF $h \rightarrow ZZ$, leptonic	0.00115	Pythia 8.306	5×10^6
$t\bar{t}h$, inclusive	0.6113 [124]	Pythia 8.306	5×10^6
$t\bar{t}W$, leptonic	0.01387×1.22	MadGraph 2.7.3	2.5×10^6
$t\bar{t}Z$, leptonic	0.00644×1.23	MadGraph 2.7.3	2.5×10^6

TABLE IV. Details of the background simulation and cross-sections

We perform an analysis of the $3l + \cancel{E}_T$ final state where we require exactly three leptons satisfying $p_T > 25, 25, 20$ GeV and $|\eta| < 2.4$, and we have put a veto on b -jets with $p_T > 30$ GeV and $|\eta| < 2.5$. In our signal benchmark, BP2, since we do not have any on-shell Z -boson, we also veto events where the invariant mass of a pair of same flavor opposite sign (SFOS) leptons lie within 10 GeV of the Z mass. After these preselections, we train our signal and background

samples using XGBOOST with a set of the following variables:

- Transverse momenta (p_T) of the three leptons
- Transverse mass (M_T) and contranverse mass (M_{CT}) of each of the three leptons with the \cancel{E}_T
- Minimum and maximum values of ΔR between opposite sign lepton pairs along with their $\Delta\eta$ values
- Invariant mass of the opposite sign lepton pairs with minimum and maximum ΔR
- Missing transverse momentum
- Number of jets in the event with the p_T of the two leading jets
- Scalar sum of p_T of all the jets in the event (H_T)
- Invariant mass of the three leptons

In benchmark BP3, we study the process $pp \rightarrow \tilde{\chi}_1^\pm \tilde{\chi}_2^0 / \tilde{\chi}_1^\pm \tilde{\chi}_3^0$, $\tilde{\chi}_1^\pm \rightarrow W^\pm \tilde{\chi}_1^0$, $\tilde{\chi}_2^0 / \tilde{\chi}_3^0 \rightarrow Z \tilde{\chi}_1^0$ with $M_{\tilde{\chi}_1^\pm} = 125.9$ GeV, $M_{\tilde{\chi}_2^0} = 155.3$ GeV, $M_{\tilde{\chi}_3^0} = 157.4$ GeV, and $M_{\tilde{\chi}_1^0} = 62.2$ GeV (benchmark 3 from Table III). For this benchmark, we apply the preselections described for BP2 above. In this benchmark, we have an on-shell Z boson in the final state. We, therefore, select those events where the invariant mass of a pair of same flavor opposite sign (SFOS) leptons lie within 10 GeV window of the Z mass, and we define these two leptons as the SFOS pair of leptons. We use the following variables for training the XGBOOST framework:

- Transverse momenta (p_T) of the three leptons
- Transverse mass (M_T) and contranverse mass (M_{CT}) of the lepton, which is not part of the SFOS pair of leptons, with the \cancel{E}_T
- ΔR and $\Delta\eta$ between the SFOS lepton pair
- $\Delta\phi$ and $\Delta\eta$ between the SFOS lepton pair system and the unpaired lepton
- $\Delta\phi$ between the SFOS lepton pair system and \cancel{E}_T
- $\Delta\phi$ between the unpaired lepton and \cancel{E}_T
- Missing transverse momentum
- Number of jets in the event with the p_T of the two leading jets
- Scalar sum of p_T of all the jets in the event (H_T)
- Invariant mass of the three leptons

We train our XGBOOST model using the following hyperparameters:

```

‘objective’:‘multi:softprob’, ‘colsample_bytree’:0.3, ‘learning_rate’:0.1,
  ‘num_class’:12, ‘max_depth’:7, ‘alpha’:5, ‘eval_metric’:‘mlogloss’,
  ‘num_round’:1000, ‘early_stopping_rounds’:3

```

We divide our total sample in two parts – one for training and one for validation. The background events are merged with a weight factor calculated using the fraction of the number of events expected at the LHC for a particular luminosity and the number of events generated for each background process. The weights are then normalised such that the sum of the weights of all the background processes becomes unity. For each epoch, we train on the training data and test the training on the validation sample. The model minimises its loss function unless the loss on the validation sample does not decrease in three consecutive iterations. The **XGBOOST** models are separately trained with 21 kinematic variables for BP2 and 18 kinematic variables for BP3. These trained models are then used to discriminate the signal benchmarks from each background class by computing the significance of observing the signal over the background events. At the $\sqrt{s} = 14$ TeV LHC with 137 fb^{-1} of integrated luminosity (\mathcal{L}), Table V shows the expected number of our two signal benchmark points and background events for a threshold of 0.9 on our **XGBOOST** output.

Number of events for $\mathcal{L} = 137 \text{ fb}^{-1}$		BP2	BP3
Backgrounds	$lll\nu$	205.6	–
	WZ , leptonic, $2j$ matched	–	46.7
	ZZ , leptonic, $2j$ matched	14.7	5.8
	$t\bar{t}$, leptonic	677.6	21.8
	VVV , inclusive	13.0	2.3
	Wh , inclusive	46.5	1.4
	Zh , inclusive	7.4	1.4
	ggF $h \rightarrow ZZ$, leptonic	2.2	0.002
	VBF $h \rightarrow ZZ$, leptonic	0.2	6.0×10^{-4}
	$t\bar{t}h$, inclusive	8.2	0.3
	$t\bar{t}W$, leptonic	9.2	0.5
	$t\bar{t}Z$, leptonic	2.5	1.0
	Total	987.1	81.2
Signal		763.4	112.1
Significance with 20% systematic uncertainty		3.1	4.5
Significance with 50% systematic uncertainty		1.3	1.98

TABLE V. Number of events from individual background processes and the signal surviving a threshold of 0.9 on the **XGBOOST** output from two models trained on benchmarks BP2 and BP3 respectively, along with the signal significance for $\mathcal{L} = 137 \text{ fb}^{-1}$.

We quote our results by assuming a 20% (50%) systematic uncertainty, where the signal significance is estimated using the formula in Ref. [125]. We present our results for $\sqrt{s} = 14$ TeV to make it easier to translate to the case of Run-3 ($\sqrt{s} = 13.6$ TeV) and HL-LHC ($\sqrt{s} = 14$ TeV) as the cross-sections for direct electroweakino production are not expected to change much. We find that the result sensitively depends on the systematic uncertainty, which can have a significant impact for light electroweakinos. Our result shows that these light Higgsinos are within the reach of LHC and could be probed with upcoming analyses of the Run-2 data or at Run-3 of the LHC, provided the systematic uncertainties can be controlled.

VII. IMPACT OF LIGHT STAUS ON THE SPECTRUM

In our previous scan, we had fixed the soft parameters related to the first and second generation squarks and all the three generations of sleptons. The former are fixed at masses around 5 TeV and the latter at masses around 2 TeV, with all the trilinear couplings associated with these squarks and sleptons set to zero. Lighter squarks and sleptons can enter various processes of the neutralino DM and affect its relic density and in turn, impact of DD experimental constraints due to the scaling factor. For squarks, as discussed previously, the strong limits from the collider searches reduce their effect on these observables. According to Ref. [62], a single non-degenerate squark has to be heavier than ~ 1200 GeV for $M_{\tilde{\chi}_1^0} \sim 60$ GeV. We have found that the presence of a 1200 GeV squark has very little effect on the relic density of DM (less than 2%) and negligible effect on the DD cross-section.

Light smuons might have important implications for the muon $g - 2$ anomaly. The observed discrepancy of the muon $g - 2$ measurement with the SM prediction requires an additional contribution of $(24.9 \pm 4.8) \times 10^{-10}$ [126, 127] from new physics. In the MSSM, the sign of the contribution to the muon $g - 2$ depends on the sign of μ . Therefore, to resolve the muon $g - 2$ anomaly within the MSSM, one prefers the positive sign of μ . In our analysis, the smuons are fixed to have a high mass around 2 TeV, therefore their contribution to the muon $g - 2$ is negligible. For the positive μ benchmark that we obtain in Sec. VI, the MSSM contribution comes to be around $\sim 2 \times 10^{-11}$, which is two orders of magnitude away from the required value. The present limit on the mass of selectrons and smuons from the CMS collaboration is $\gtrsim 700$ GeV for a 60 GeV $\tilde{\chi}_1^0$ [49]. When we reduce the smuon mass parameters (both $M_{\tilde{L}_{2L}}$ and $M_{\tilde{e}_{2R}}$) in the positive μ benchmark from 2 TeV to 700 GeV, the MSSM contribution becomes 4.4×10^{-11} , which is still not enough to explain the observation.

Among the three generations of sleptons, staus have the weakest limits [66]. As motivated earlier in Section II, for light staus, we are more interested in studying the effect of RH light stau – for this we vary the parameter $M_{\tilde{e}_{3R}}$ from 85 GeV to 500 GeV. We find that the present searches of stau leptons at the LHC, which are already recasted in the SModelS package, do not constrain the scenario of RH staus as the NLSP for the DM mass range under consideration, as shown in Fig. 24 of Appendix B.

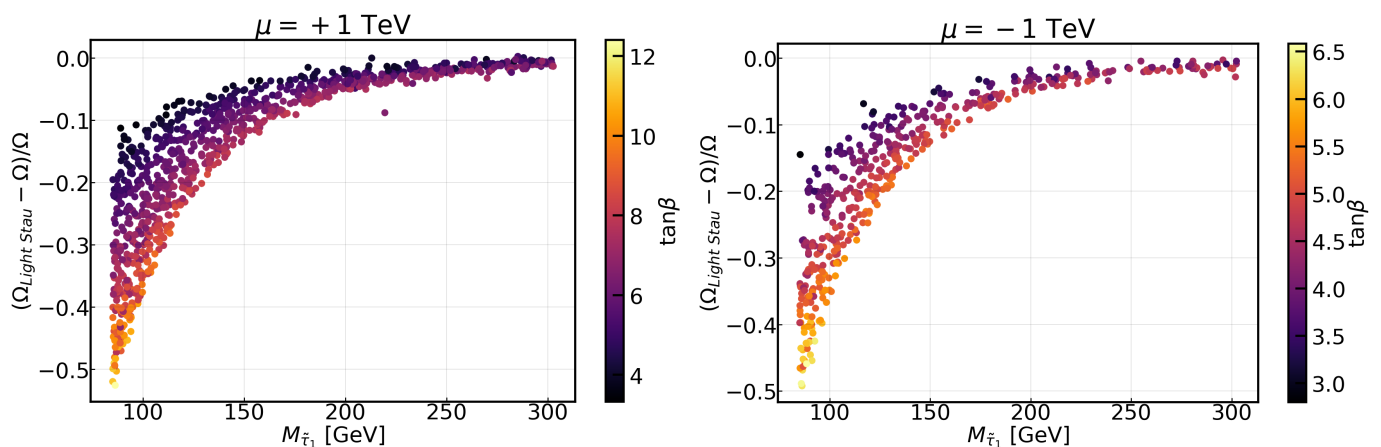


FIG. 16. Fractional change in the relic density of the LSP with and without light RH staus as a function of the mass of the lightest stau for $\mu = +1$ TeV (left) and $\mu = -1$ TeV (right). These parameter points survive all the constraints described earlier and the *colorbar* shows the $\tan \beta$ of these points.

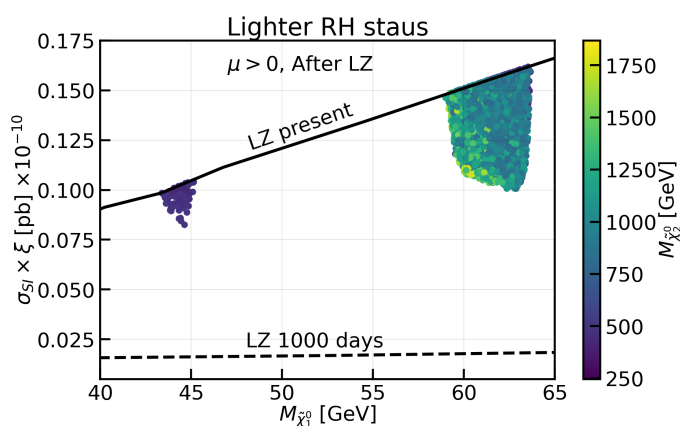


FIG. 17. Scaled SI DM-nucleon cross-section ($\sigma_{SI} \times \xi$) for $\mu > 0$, with light RH staus ($M_{\tilde{e}_{3R}} = 85$ GeV), as a function of the mass of the LSP neutralino DM in the region of parameter space satisfying LEP, flavor, Higgs constraints, relic density, and DM DD constraints from the XENON-1T, PICO-60, PandaX-4T, and LZ experiments, defined as “**After LZ**”.

Since light RH staus are still allowed by the collider constraints, we study their impact on the relic density of the Bino-like LSP that we have studied so far. We observe that for lighter Higgsinos, the couplings $g_{Z\tilde{\chi}_1^0\tilde{\chi}_1^0}$ and $g_{h\tilde{\chi}_1^0\tilde{\chi}_1^0}$ are larger, therefore, we do not expect a large effect from lighter RH staus. For heavier Higgsinos, say having $|\mu| = 1$ TeV, these couplings have small values due to reduced Higgsino components in the lightest neutralino, and the effect of light RH stau becomes important. To demonstrate this, Fig. 16 shows the fraction of change in the relic density of the LSP DM with and without light RH staus for varying masses of the lightest stau for both positive (*left*) and negative (*right*) μ , with the Higgsino mass parameter having a value of 1 TeV in the h funnel. We observe that the sign of μ does not play a significant role, and light staus of 100 GeV can reduce the relic density by 30-40%.

To maximize the effect of a light stau, we fix $M_{\tilde{e}_{3R}} = 85$ GeV corresponding to $M_{\tilde{\tau}_1} = 90-95$ GeV, a value above the LEP bound [128–133]. We then redo the scan to examine the impact of adding the light stau on the parameter space of the light neutralino thermal dark matter. Fig. 17 shows the allowed parameter space with the “After LZ” set of cuts in the $\sigma_{SI} \times \xi - M_{\tilde{\chi}_1^0}$ plane for $\mu > 0$. We observe that the light stau reduces the relic density and lowers the scaled SI DD cross-sections, allowing a small region of parameter space in the Z funnel. It also extends the allowed region in the h funnel to lower cross sections. Both the Z and h funnels are within the reach of the LZ projected sensitivity with 1000 days of data.

Our analysis is for a 100% branching fraction of Higgsinos to the WZ final state. Experimental collaborations also quote their exclusion boundaries assuming 100% branching to a specific final state and a particular mass hierarchy. The prospects of the presence of other light SUSY particles might also affect the collider constraints on Higgsinos, if the latter decay into the former with significant branching fractions. One such possibility which we mention in our paper is the presence of light staus having masses between the Bino-like LSP and Higgsinos, which are still allowed by the searches at LHC [66] (also see Fig. 24 in Appendix B).

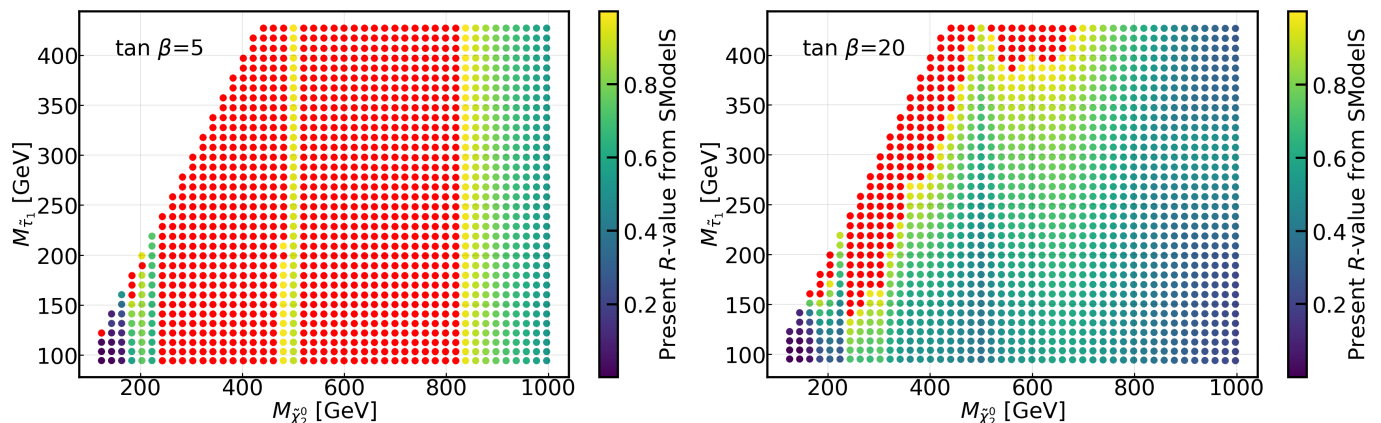


FIG. 18. SModelS R -values in the plane of mass of the Higgsino-like neutralino and the lightest stau, which is RH, for a range of masses where the Higgsino can kinematically decay to final states involving stau leptons for $\tan \beta = 5$ (*left*) and $\tan \beta = 20$ (*right*). The points marked in *red* are already excluded.

In order to study the impact of light staus on the exclusion limit of Higgsinos, we perform a scan over the Higgsino-RH stau parameter space, where we fix the Bino mass parameter at 60 GeV and vary μ in the range [100-1000] GeV and $M_{\tilde{e}_{3R}}$ in the range [85-500] GeV. Fig. 18 shows the R -values of the present analyses as implemented in SModelS in the plane of mass of the Higgsino-like neutralino and the lightest stau. We present the result for a range of masses where the Higgsino can kinematically decay to final states involving stau leptons for $\tan \beta = 5$ (*left*) and $\tan \beta = 20$ (*right*). The points marked in *red* are already excluded, i.e., have a R -value greater than unity⁸. We observe that

⁸ There is a narrow allowed band around Higgsino masses of 500 GeV in the *left panel* of Fig. 18, where all the points have R -values greater than 0.9. These are very close to the exclusion limit. This region falls in the gap of two separate analyses – CMS-SUS-20-001 [49] and ATLAS-SUSY-2018-41 [51]. The first analysis involves leptons in the final state sensitive to smaller Higgsino masses, while the second one uses boosted hadronically decaying bosons, which is sensitive to higher masses.

the presence of such light staus affect the exclusion limit of Higgsino NLSPs. The impact of light RH staus become stronger for higher $\tan\beta$ values where the branching of Higgsinos to stau leptons increase, thereby, weakening the result.

Benchmarks with light staus (<i>mass parameters in GeV</i>)			$M_h [\Delta_{M_h}^{FH}]$ [GeV]	$\sigma_{SI} \times \xi \times 10^{-10}$ [pb]	
$\mu < 0$	Z-funnel	BP5	$M_t = 173.21, M_1 = 44, M_2 = 2000, \mu = -124, \tan\beta = 5, M_A = 3000,$ $M_{\tilde{Q}_{3L}} = M_{\tilde{t}_R} = M_{\tilde{b}_R} = A_t = 10000, M_3 = 3000, M_{\tilde{e}_{3R}} = 85$	125.86[±0.96]	7.45×10^{-4}
	<i>h</i> -funnel	BP6	$M_t = 173.21, M_1 = 68, M_2 = 2000, \mu = -150, \tan\beta = 50, M_A = 3000,$ $M_{\tilde{Q}_{3L}} = M_{\tilde{t}_R} = M_{\tilde{b}_R} = 5000, A_t = -5000, M_3 = 3000, M_{\tilde{e}_{3R}} = 85$	125.65[±0.63]	0.137
$\mu > 0$	Z-funnel	BP7	$M_t = 173.21, M_1 = 44, M_2 = 2000, \mu = 500, \tan\beta = 50, M_A = 6000,$ $M_{\tilde{Q}_{3L}} = M_{\tilde{t}_R} = M_{\tilde{b}_R} = 4500, A_t = 4000, M_3 = 5000, M_{\tilde{e}_{3R}} = 85$	125.11[±0.99]	0.095
	<i>h</i> -funnel	BP8	$M_t = 173.21, M_1 = 62, M_2 = 2000, \mu = 500, \tan\beta = 20, M_A = 6000,$ $M_{\tilde{Q}_{3L}} = M_{\tilde{t}_R} = M_{\tilde{b}_R} = 4500, A_t = 4000, M_3 = 5000, M_{\tilde{e}_{3R}} = 150$	124.77[±0.97]	0.152

TABLE VI. Parameters corresponding to four benchmark points satisfying all the present constraints from the $\mu > 0$ and $\mu < 0$ scenarios along with their scaled SI DD cross-sections. The mass of the Higgs boson M_h and the uncertainty in M_h computed by FeynHiggs ($\Delta_{M_h}^{FH}$) are also shown.

Subsequently, we study the prospect of a XGBOOST based analysis for benchmark points where we have a light stau, which are still allowed by the SUSY searches implemented in SModelS-2.3.0. We select four benchmarks – from the Z and h funnel regions of $\mu > 0$ and $\mu < 0$, each. These are listed in Table VI with the relevant soft parameters. BP5 and BP6 correspond to the light Higgsino benchmarks studied in the previous section (BP2 and BP3 in Table III) to which we add a light stau with a physical mass around 90 GeV. Due to light RH staus, a region of parameter space in the previously excluded Z funnel for positive μ opens up, and survives both LZ and electroweakino direct search bounds. We select a benchmark from this region, called BP7, with moderate Higgsino mass around 500 GeV and a very light stau with $M_{\tilde{e}_{3R}} = 85$ GeV. For the h funnel of $\mu > 0$, Higgsinos up to 850 GeV masses were excluded for a 100% branching to the LSP. If RH staus are brought below the Higgsino, then Higgsinos around 500 GeV masses can still satisfy the collider limits for particular masses of the RH stau, like with $M_{\tilde{e}_{3R}} = 150$ GeV, which we choose as BP8.

Number of events for $\mathcal{L} = 300 \text{ fb}^{-1}$		BP5	BP6
Backgrounds	$lll\nu$	190.7	105.6
	ZZ , leptonic, $2j$ matched	39.4	26.5
	$t\bar{t}$, leptonic	3500.0	1520.5
	VVV , inclusive	14.9	7.1
	Wh , inclusive	61.0	27.7
	Zh , inclusive	22.8	13.5
	ggF $h \rightarrow ZZ$, leptonic	1.2	0.5
	VBF $h \rightarrow ZZ$, leptonic	0.2	0.05
	$t\bar{t}h$, inclusive	11.0	6.4
	$t\bar{t}W$, leptonic	4.7	2.1
	$t\bar{t}Z$, leptonic	2.4	1.4
Total	3848.3	1711.4	
Signal	5937.9	3513.9	
Significance with 20% systematic uncertainty	5.51	6.81	
Significance with 50% systematic uncertainty	2.21	2.74	

TABLE VII. Number of events from individual background processes and the signal surviving a threshold of 0.9 on the XGBOOST output from two models trained on benchmarks BP5 and BP6, respectively, along with the signal significance for $\mathcal{L} = 300 \text{ fb}^{-1}$.

When the Higgsino decays to staus, we have final states enriched with tau leptons. They in turn decay to electrons, muons, or pions. In our analysis for these benchmarks, we perform a similar analysis like the $3l$ +MET, including the hadronic decays of the tau leptons. Table VII shows the expected number of our signal benchmark points BP5 and

Number of events for $\mathcal{L} = 300 \text{ fb}^{-1}$		BP7	BP8
Backgrounds	$ll\nu$	40.1	35.7
	ZZ , leptonic, $2j$ matched	4.9	3.43
	$t\bar{t}$, leptonic	1860.1	1659.2
	VVV , inclusive	16.7	16.6
	Wh , inclusive	13.8	10.5
	Zh , inclusive	3.0	2.1
	ggF $h \rightarrow ZZ$, leptonic	0.02	0.02
	VBF $h \rightarrow ZZ$, leptonic	0.004	0.004
	$t\bar{t}h$, inclusive	12.6	10.6
	$t\bar{t}W$, leptonic	8.7	9.2
	$t\bar{t}Z$, leptonic	2.7	2.8
	Total	1962.6	1750.0
Signal		406.8	170.2
Significance with 5% systematic uncertainty		3.56	1.70
Significance with 10% systematic uncertainty		1.90	0.92

TABLE VIII. Number of events from individual background processes and the signal surviving a threshold of 0.98 on the XGBOOST output from two models trained on benchmarks BP7 and BP8, respectively, along with the signal significance for $\mathcal{L} = 300 \text{ fb}^{-1}$.

BP6 along with the background events for a threshold of 0.9 on our XGBOOST output. We also quote the significance by assuming a 20% (50%) systematic uncertainty. We find that both BP5 and BP6, belonging to the $\mu < 0$ scenario, can be probed with our analysis at the Run-3 of the LHC using 300 fb^{-1} of data, with a signal significance $\gtrsim 2\sigma$, despite a large systematic uncertainty of 50%. For positive μ , the two benchmarks have higher Higgsino masses (500 GeV), and therefore, lower production cross-sections. Hence, we put a stronger XGBOOST threshold to reduce the backgrounds further. Table VIII shows the expected number of our signal benchmark points BP7 and BP8 along with the background events for a threshold of 0.98 on our XGBOOST output. For heavier Higgsinos, the systematic uncertainties might be much smaller. We, therefore, quote the significance by assuming a 5% (10%) systematic uncertainty. For BP7, we find that if the uncertainty can be brought down to 5%, we can achieve more than 3σ significance, while for BP8, we require the uncertainty to be around 2% to have 3σ significance.

VIII. THE THERMAL NEUTRALINO IN NON-STANDARD COSMOLOGY

Until now, we have worked within the framework of standard cosmological scenario. However, if the neutralino DM is produced thermally in a non-standard cosmology, then the relic density constraint can be relaxed. This can happen, for example, due to entropy injection in the Universe from the late decay of some particle after the DM freezes out. In this scenario, even if the relic density of the DM at freeze-out is much larger than the present observed relic, it can be diluted due to the increase in the entropy density of the Universe. Ref. [134, Fig. 8] shows that for a mass of WIMP DM in the range 40-60 GeV, the quantity $\langle\sigma v\rangle$, which is the annihilation cross-section multiplied by the DM velocity, can be reduced from the usual value of 10^{-9} GeV^{-2} in standard cosmological scenarios to a value below $10^{-15} \text{ GeV}^{-2}$ in non-standard cosmologies. Therefore, in the non-standard cosmology, we can allow for very small DM annihilation cross-sections. The allowed parameter space is not restricted to the funnel regions and the Higgsinos can have masses as large as 2 TeV, or even heavier in both the Z and h funnels. Having very small couplings, these points will also satisfy the DD bounds and therefore, will provide interesting benchmarks for probing non-standard cosmologies. Fig. 19 shows the parameter space surviving the LEP, flavor, Higgs and DM DD constraints in the mass and relic density of the LSP plane, with the colorbar showing the mass of $\tilde{\chi}_2^0$.

Fig. 20 shows the scaled SI DD cross-section as a function of the DM mass for scenarios where DM is found to be

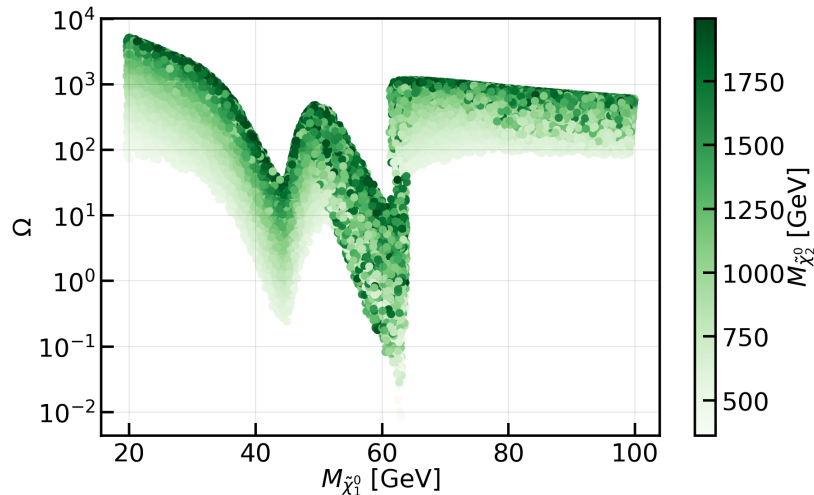


FIG. 19. The relic density at freeze-out of the LSP neutralino DM as a function of its mass (x -axis) and the mass of the Higgsino-like $\tilde{\chi}_2^0$ (*colorbar*), in the region of parameter space satisfying LEP, flavor, Higgs constraints, and DM DD constraints from the XENON-1T, PICO-60, PandaX-4T, and LZ experiments. It is assumed that entropy injection in non-standard cosmology can reduce the relic density of overabundant DM.

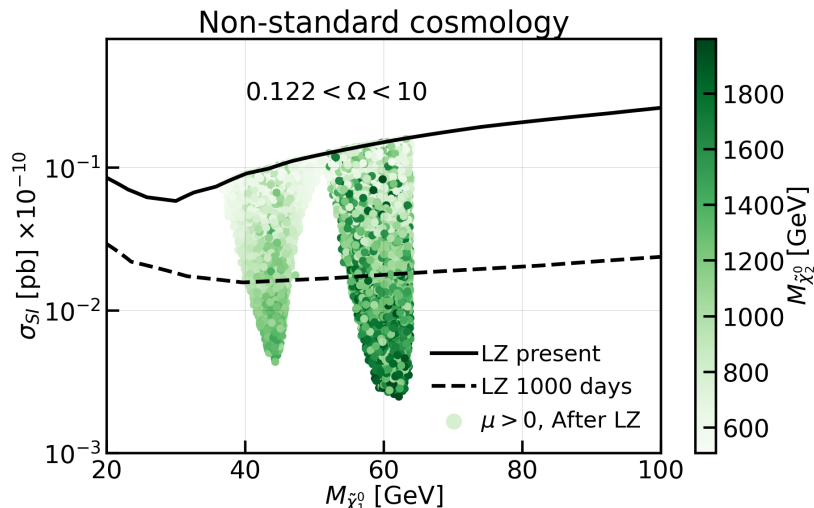


FIG. 20. Scaled SI DM-nucleon cross-section ($\sigma_{SI} \times \xi$) for $\mu > 0$ in the non-standard cosmological scenario, where the entropy dilution can provide the correct observed DM relic density upto a freeze-out density of around 10, as a function of the mass of the LSP neutralino DM in the region of parameter space satisfying LEP, flavor, Higgs constraints, relic density ($0.122 < \Omega < 10$), and DM DD constraints from the XENON-1T, PICO-60, PandaX-4T, and LZ experiments.

overabundant in the standard cosmological scenario, but can satisfy the observed relic density due to non-standard cosmology. We apply all the constraints from the set “After LZ”, where only the relic density constraint is modified to $0.122 < \Omega h^2 < 10$, where we assume that the non-standard cosmology can dilute the DM relic density by a factor of about 100. We observe that new regions of the parameter space now survive the experimental constraints, in both the Z and h funnel regions. This would allow us to identify scenarios of non-standard cosmology, depending on the nature of the observed signals. For instance, if one observes DM in the Z -funnel region and simultaneously a LHC signal for Higgsinos heavier than 500 GeV, it might indicate non-standard cosmology with thermal production of the neutralino DM. Even in the h -funnel region, we have an idea of the minimum DD cross-section values that can survive in standard cosmology. Observing a signal with the future LZ data might hint towards a non-standard cosmological

picture.

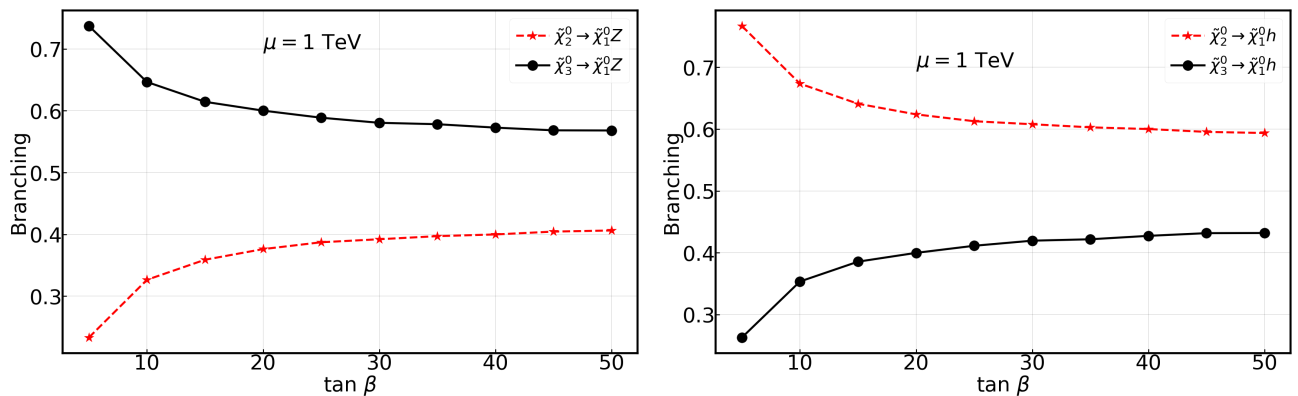


FIG. 21. Branching fractions of the two Higgsino-like neutralinos with $\mu = 1$ TeV to $\tilde{\chi}_1^0 Z$ (*left*) and $\tilde{\chi}_1^0 h$ (*right*) when the staus are heavy.

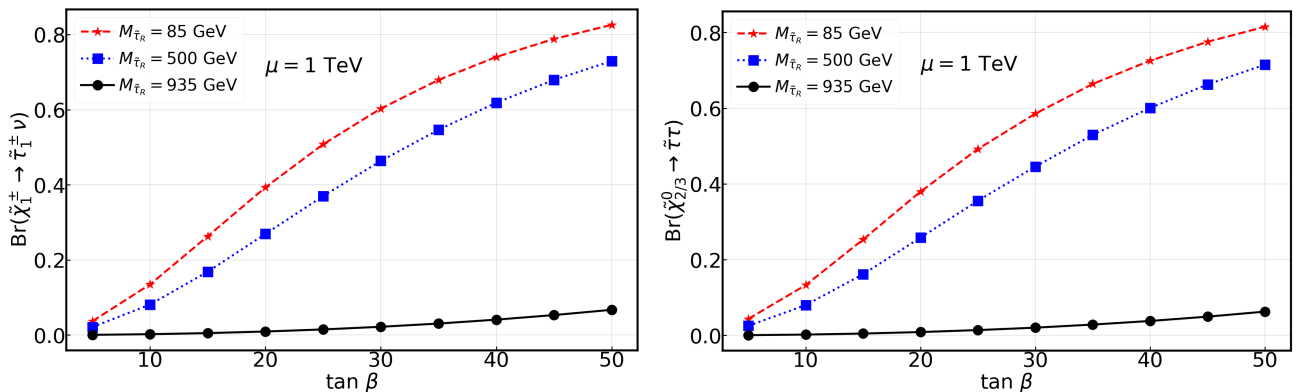


FIG. 22. Branching fractions of the Higgsino-like chargino (*left*) and the two neutralinos (*right*) to final states involving various masses of RH staus.

Additionally, for a DM signal from DD experiments in the h funnel, it is interesting to explore whether collider experiments can provide any hint of non-standard cosmology. If we observe a signal for heavy Higgsinos, having masses around a TeV for high $\tan\beta$, then it might suggest a non-standard cosmological scenario. To answer the question whether we can get an idea of the $\tan\beta$ value from the signal, we studied the variation in branching of the Higgsinos to various final states as a function of $\tan\beta$. Fig. 21 shows the branching of the neutral Higgsinos to the LSP and Z/h. We find that although there is a $\tan\beta$ dependence, the sum of $\text{Br}(\tilde{\chi}_2^0 \rightarrow \tilde{\chi}_1^0 Z) + \text{Br}(\tilde{\chi}_3^0 \rightarrow \tilde{\chi}_1^0 Z)$ (or with Higgs boson in the final state), has no variation with $\tan\beta$. Therefore, it won't be possible to estimate the $\tan\beta$ value from the branching fraction of Higgsinos to these final states. We then turn to the case of light staus, such that the staus have masses between the Bino and the Higgsinos. Fig. 22 shows the branching of the chargino and the two neutralinos decaying to stau and tau for three different stau masses. We observe a very clear $\tan\beta$ dependence in this case, especially for lighter staus. If we observe a signal of Higgsinos and could identify the final state with staus, we can get an idea of the $\tan\beta$ from the branching fraction of Higgsinos decaying to staus. The branching to staus is higher for high $\tan\beta$, where relic density cannot be satisfied for a TeV scale Higgsino within standard cosmology, and therefore, points toward a non-standard cosmological scenario.

IX. CONCLUSION

In summary, this study shows that the current experiments, especially the recent results from electroweakino searches at the LHC and dark matter DD measurements from LZ, have severely constrained the $\mu > 0$ scenario for a light neutralino thermal DM in the pMSSM with 10 free parameters. The DD result of the LZ collaboration is a strong constraint and it affects different regions of the parameter space in the pMSSM depending on the constructive and destructive interferences between the light and the heavy CP-even neutral Higgs bosons. For heavy staus, the Z -funnel is completely excluded, and only heavy Higgsinos ($M_{\tilde{\chi}_1^0} \gtrsim 850$ GeV) are allowed in the h -funnel region. In the $\mu < 0$ scenario of the same model, the allowed parameter space consists of either Higgsinos heavier than ~ 850 GeV in the h -funnel or restricted to a narrow region of light Higgsinos having mass of 125-160 GeV in the Z and h -funnels, unlike the $\mu > 0$ scenario. For light Higgsinos, there is a constructive interference between the h and H contributions to the DD cross-section for positive μ . Therefore, it is not possible to evade the LZ bounds. There is a destructive interference between the contributions from the two CP-even neutral Higgs bosons for negative μ , thereby, opening up allowed parameter space with light Higgsinos. Our XGBOOST analysis with the $3l$ +MET signature shows that these light Higgsinos could be probed with the Run-2 data of 137 fb^{-1} , if the systematic uncertainties lie within 20-30%. These benchmarks are still allowed by the available recasting frameworks, like SModelS and CheckMATE, which can translate the result of Wino-like NLSPs, provided by experimental collaborations, for Higgsino-like NLSPs. Thus, they form an important target for Run-3 searches. We also find that the DM bounds on the relic density and the DD SI cross-sections severely constrain any simplified extension of SM with a Majorana fermionic DM coupling only to the discovered Higgs boson.

The situation changes when we have light RH staus as NLSPs. They provide an additional annihilation channel for the DM and, therefore, reduce the relic density by a factor depending on the mass of the stau. Furthermore, they also affect the exclusion limits of Higgsinos in collider searches, when the Higgsino can decay to staus with significant branching fractions. Due to both these effects, we get an allowed region of parameter space even in the Z funnel of $\mu > 0$ with lighter staus. In the h funnel of positive μ , the presence of light staus relax the lower limit on Higgsino masses, and 500 GeV Higgsinos are still allowed in such a scenario. Our preliminary analysis of these benchmarks shows they are accessible at Run-3 of LHC if the systematic uncertainties can be controlled. The future direct detection experiments, e.g., 1000 days of LZ, can probe the Z and the h funnels with light staus, as can be seen from Fig. 17. The status further changes when we go to non-standard cosmological scenarios, where the relic density can be satisfied by late injection of entropy in the Universe. Therefore, a large region of the parameter space becomes available. We discuss some ways to identify a non-standard history of our Universe from the combination of signals in future DM DD and collider experiments, which could not be realised assuming the standard cosmological model. The future DM DD experiments and the LHC Run-3 have promising prospects in exploring the remaining corners of the pMSSM parameter space with a light neutralino thermal dark matter.

ACKNOWLEDGEMENT

We thank Sabine Kraml for the useful discussion and help related to the SModelS package. The work of G.B. and R.M.G. was funded in part by the Indo-French Centre for the Promotion of Advanced Research, Grant no: 6304-2. R.M.G. wishes to acknowledge the support of Indian National Science Academy under the award of INSA Senior Scientist Scheme. The work of B.B. was supported by the SERB Core Research Grant CRG/2022/001922 and the SERB Matrics Grant MTR/2022/000264. B.B. and R.S. thank Prabhat Solanki and Camellia Bose for useful discussions. The work of R.K.B. was supported by the World Premier International Research Center Initiative (WPI), MEXT, Japan. R.K.B. thanks the U.S. Department of Energy for the financial support under grant number DE-SC0016013. R.S. acknowledges the support of the Deutsche Forschungsgemeinschaft (DFG) through the funds provided to the Sino-German Collaborative Research Center TRR110 ‘‘Symmetries and the Emergence of Structure

in QCD” (DFG Project-ID 196253076)”. R.S. would like to thank the Indian Institute of Science for computational support.

Appendix A: Impact of the constraints on the invisible branching of the Higgs boson

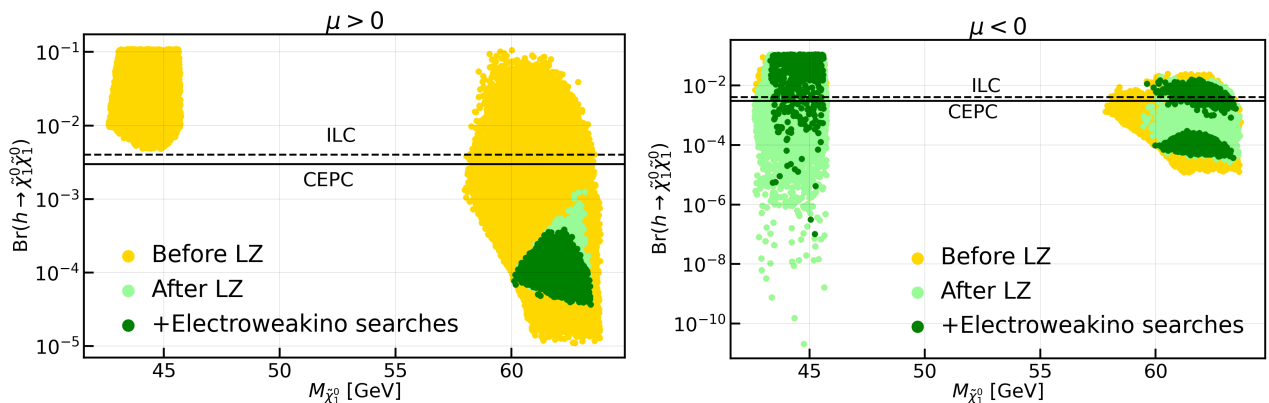


FIG. 23. Allowed region of parameter space in the $M_{\tilde{\chi}_1^0}$ - $\text{Br}(h \rightarrow \tilde{\chi}_1^0 \tilde{\chi}_1^0)$ plane for $\mu > 0$ (left) and $\mu < 0$ (right) with all the constraints 'Before LZ' (yellow), 'After LZ' (light green), and from electroweakino searches (dark green). Dashed and solid black lines show the projected sensitivity for $\text{Br}(h \rightarrow \tilde{\chi}_1^0 \tilde{\chi}_1^0)$ from the ILC and CEPC experiments, respectively.

Appendix B: Collider limit on right-handed staus

Fig. 24 shows the R -values of present analyses searching for stau leptons at the LHC, as recasted by the `SModelS` package in the plane of mass of the lightest stau which is RH, $M_{\tilde{\tau}_1}$ and the mass of the lightest neutralino which is Bino-like, $M_{\tilde{\chi}_1^0}$ for a Higgsino mass parameter of 1 TeV. We observe that the R -values are all less than unity, implying that the current analyses are not sensitive to this region of parameter space. As a result, light staus in the mass range of 90-400 are still allowed, the lower limit coming from the LEP experiment [128]. We translate these R -values with the square root of luminosity for the future runs of LHC. We find that Run-3 with 300 fb^{-1} integrated luminosity will be sensitive to a small region of parameter space for $M_{\tilde{\chi}_1^0} \lesssim 20 \text{ GeV}$ and $M_{\tilde{\tau}_1}$ between 200-250 GeV, and the HL-LHC run with 3 ab^{-1} of luminosity will be able to probe this whole region of parameter space.

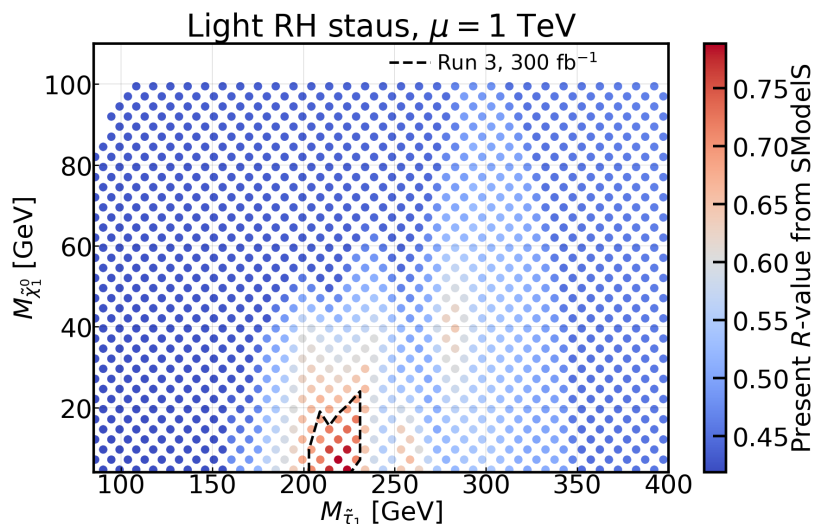


FIG. 24. `SmodelS` R -values of present analyses searching for stau leptons at the LHC in the $M_{\tilde{\tau}_1}$ - $M_{\tilde{\chi}_1^0}$ plane, where the lightest stau is RH and $M_{\tilde{\chi}_1^0}$ is Bino-like for $\mu = 1 \text{ TeV}$.

Appendix C: Combination of analyses in SModelS

A new important feature in SModelS-2.3 [120] is the possibility to combine multiple search analyses. The combination of analyses assumes that these analyses are uncorrelated and therefore, has to be used carefully. One of the difficulties in using this option is that the names of the analyses that have to be combined should be given as an input. For a particular point in parameter space, it is not always clear beforehand which analyses are important and whether they can be combined consistently. Another technical challenge is that signal regions within an analysis cannot be combined when one chooses to combine analyses within the current version of SModelS. Nevertheless, it is important to check the effect of combining the most sensitive analyses, at least for the benchmark points, to ascertain whether or not they are excluded.

Table IX shows the comparison of the R -values when combining the most sensitive analyses for the benchmark points with the ones obtained without combining the analyses. For each case, we also show the names of the most sensitive analyses.

For BP1 and BP4, which correspond to the heavy higgsinos in the $\mu > 0$ and $\mu < 0$ scenarios, we find that the R -value decreases when we combine the most sensitive analyses. This happens in all cases where the combination of signal regions is more important than combining analyses since both combination cannot be done simultaneously. For BP1 and BP4, the ATLAS-SUSY-2018-41 analysis is sensitive to different topologies and gains significantly in sensitivity when combining signal regions.

For BP2 and BP3, there are very slight changes in the R -values when we combine the analyses. For BP5, BP7 and BP8, the R -values are very small to begin with, on combining the analyses the R -value increases slightly for BP5, but degrades for BP7 and BP8. Lastly, for BP6, which is the stau benchmark in the $\mu < 0$ h -funnel, we find that combining the analyses increases the R -value significantly – from 0.599 to 0.887. We conclude that none of our benchmark points are excluded after we apply the combination of analyses.

Benchmarks	Without combination of analyses		With combination of analyses	
	Analysis	R -value	Analyses	R -value
BP1	ATLAS-SUSY-2018-41	0.815	ATLAS-SUSY-2018-05-ewk ATLAS-SUSY-2018-41 ATLAS-SUSY-2019-08 CMS-SUS-16-039-agg CMS-SUS-21-002	0.615
BP2	ATLAS-SUSY-2013-11	0.141	ATLAS-SUSY-2013-11 ATLAS-SUSY-2019-02 CMS-SU-13-012	0.144
BP3	ATLAS-SUSY-2019-09	0.443	ATLAS-SUSY-2013-11 ATLAS-SUSY-2019-02 ATLAS-SUSY-2019-09 CMS-SUS-13-012	0.402
BP4	ATLAS-SUSY-2018-41	0.805	ATLAS-SUSY-2018-05-ewk ATLAS-SUSY-2018-41 ATLAS-SUSY-2019-08 CMS-SUS-16-039-agg CMS-SUS-21-002	0.614
BP5	ATLAS-SUSY-2018-05-ewk	0.059	ATLAS-SUSY-2016-24 ATLAS-SUSY-2017-03 ATLAS-SUSY-2018-05-ewk ATLAS-SUSY-2018-41 ATLAS-SUSY-2019-09 CMS-SUS-21-002	0.078
BP6	ATLAS-SUSY-2018-05-ewk	0.599	ATLAS-SUSY-2016-24 ATLAS-SUSY-2017-03 ATLAS-SUSY-2018-05-ewk ATLAS-SUSY-2018-41 ATLAS-SUSY-2019-09 CMS-SUS-21-002	0.887
BP7	ATLAS-SUSY-2013-12	0.061	ATLAS-SUSY-2013-11 ATLAS-SUSY-2019-02 CMS-SUS-13-012	0.023
BP8	ATLAS-SUSY-2019-09	1.16×10^{-3}	ATLAS-SUSY-2019-02 ATLAS-SUSY-2019-09 CMS-SUS-13-012	9.37×10^{-4}

TABLE IX. Comparison of the R -values from the latest version of `SModelS` (database 2.3.0) on our eight benchmark points without and with the combination of the most sensitive analyses for each point. When not combining analyses, signal regions within an analysis could be combined, which cannot be done when combining analyses.

-
- [1] **ATLAS** Collaboration, G. Aad *et al.*, “Interpretations of the ATLAS measurements of Higgs boson production and decay rates and differential cross-sections in pp collisions at $\sqrt{s} = 13$ TeV,” [arXiv:2402.05742 \[hep-ex\]](#).
- [2] **CMS** Collaboration, A. Tumasyan *et al.*, “A search for decays of the Higgs boson to invisible particles in events with a top-antitop quark pair or a vector boson in proton-proton collisions at $\sqrt{s} = 13$ TeV,” *Eur. Phys. J. C* **83** no. 10, (2023) 933, [arXiv:2303.01214 \[hep-ex\]](#).
- [3] S. Weinberg, “Implications of Dynamical Symmetry Breaking,” *Phys. Rev. D* **13** (1976) 974–996. [Addendum: *Phys.Rev.D* 19, 1277–1280 (1979)].
- [4] E. Gildener and S. Weinberg, “Symmetry Breaking and Scalar Bosons,” *Phys. Rev. D* **13** (1976) 3333.
- [5] L. Susskind, “Dynamics of spontaneous symmetry breaking in the weinberg-salam theory,” *Phys. Rev. D* **20** (Nov, 1979) 2619–2625. <https://link.aps.org/doi/10.1103/PhysRevD.20.2619>.
- [6] **L3** Collaboration, M. Acciarri *et al.*, “Search for charginos and neutralinos in e^+e^- collisions at $\sqrt{S} = 189$ -GeV,” *Phys. Lett. B* **472** (2000) 420–433, [arXiv:hep-ex/9910007](#).
- [7] **OPAL** Collaboration, G. Abbiendi *et al.*, “Search for chargino and neutralino production at $s^{*(1/2)} = 192$ -GeV to 209 GeV at LEP,” *Eur. Phys. J. C* **35** (2004) 1–20, [arXiv:hep-ex/0401026](#).
- [8] **Planck** Collaboration, N. Aghanim *et al.*, “Planck 2018 results. VI. Cosmological parameters,” *Astron. Astrophys.* **641** (2020) A6, [arXiv:1807.06209 \[astro-ph.CO\]](#). [Erratum: *Astron.Astrophys.* 652, C4 (2021)].
- [9] K. Griest and H. E. Haber, “Invisible decays of higgs bosons in supersymmetric models,” *Phys. Rev. D* **37** (Feb, 1988) 719–728. <https://link.aps.org/doi/10.1103/PhysRevD.37.719>.
- [10] A. Djouadi, P. Janot, J. Kalinowski, and P. M. Zerwas, “SUSY decays of Higgs particles,” *Phys. Lett. B* **376** (1996) 220–226, [arXiv:hep-ph/9603368](#).
- [11] G. Belanger, F. Boudjema, F. Donato, R. Godbole, and S. Rosier-Lees, “SUSY Higgs at the LHC: Effects of light charginos and neutralinos,” *Nucl. Phys. B* **581** (2000) 3–33, [arXiv:hep-ph/0002039](#).
- [12] G. Belanger, F. Boudjema, A. Cottrant, R. M. Godbole, and A. Semenov, “The MSSM invisible Higgs in the light of dark matter and g-2,” *Phys. Lett. B* **519** (2001) 93–102, [arXiv:hep-ph/0106275](#).
- [13] D. Hooper and T. Plehn, “Supersymmetric dark matter: How light can the LSP be?,” *Phys. Lett. B* **562** (2003) 18–27, [arXiv:hep-ph/0212226](#).
- [14] J. Hisano, S. Matsumoto, and M. M. Nojiri, “Unitarity and higher order corrections in neutralino dark matter annihilation into two photons,” *Phys. Rev. D* **67** (2003) 075014, [arXiv:hep-ph/0212022](#).
- [15] G. Belanger, F. Boudjema, A. Cottrant, A. Pukhov, and S. Rosier-Lees, “Lower limit on the neutralino mass in the general MSSM,” *JHEP* **03** (2004) 012, [arXiv:hep-ph/0310037](#).
- [16] H. K. Dreiner, S. Heinemeyer, O. Kittel, U. Langenfeld, A. M. Weber, and G. Weiglein, “Mass Bounds on a Very Light Neutralino,” *Eur. Phys. J. C* **62** (2009) 547–572, [arXiv:0901.3485 \[hep-ph\]](#).
- [17] D. Albornoz Vasquez, G. Belanger, C. Boehm, A. Pukhov, and J. Silk, “Can neutralinos in the MSSM and NMSSM scenarios still be light?,” *Phys. Rev. D* **82** (2010) 115027, [arXiv:1009.4380 \[hep-ph\]](#).
- [18] L. Calibbi, T. Ota, and Y. Takahashi, “Light Neutralino in the MSSM: a playground for dark matter, flavor physics and collider experiments,” *JHEP* **07** (2011) 013, [arXiv:1104.1134 \[hep-ph\]](#).
- [19] A. Choudhury and A. Datta, “Many faces of low mass neutralino dark matter in the unconstrained MSSM, LHC data and new signals,” *JHEP* **06** (2012) 006, [arXiv:1203.4106 \[hep-ph\]](#).
- [20] A. Arbey, M. Battaglia, and F. Mahmoudi, “Light Neutralino Dark Matter in the pMSSM: Implications of LEP, LHC and Dark Matter Searches on SUSY Particle Spectra,” *Eur. Phys. J. C* **72** (2012) 2169, [arXiv:1205.2557 \[hep-ph\]](#).
- [21] H. K. Dreiner, J. S. Kim, and O. Lebedev, “First LHC Constraints on Neutralinos,” *Phys. Lett. B* **715** (2012) 199–202, [arXiv:1206.3096 \[hep-ph\]](#).
- [22] C. Boehm, P. S. B. Dev, A. Mazumdar, and E. Pukartas, “Naturalness of Light Neutralino Dark Matter in pMSSM after LHC, XENON100 and Planck Data,” *JHEP* **06** (2013) 113, [arXiv:1303.5386 \[hep-ph\]](#).
- [23] A. Choudhury and A. Datta, “Neutralino dark matter confronted by the LHC constraints on Electroweak SUSY signals,” *JHEP* **09** (2013) 119, [arXiv:1305.0928 \[hep-ph\]](#).
- [24] B. Ananthanarayan, J. Lahiri, P. N. Pandita, and M. Patra, “Invisible decays of the lightest Higgs boson in supersymmetric models,” *Phys. Rev. D* **87** no. 11, (2013) 115021, [arXiv:1306.1291 \[hep-ph\]](#).
- [25] L. Calibbi, J. M. Lindert, T. Ota, and Y. Takahashi, “Cornering light Neutralino Dark Matter at the LHC,” *JHEP* **10** (2013) 132, [arXiv:1307.4119 \[hep-ph\]](#).

- [26] G. Bélanger, G. Drieu La Rochelle, B. Dumont, R. M. Godbole, S. Kraml, and S. Kulkarni, “LHC constraints on light neutralino dark matter in the MSSM,” *Phys. Lett. B* **726** (2013) 773–780, [arXiv:1308.3735 \[hep-ph\]](#).
- [27] M. Chakraborti, U. Chattopadhyay, A. Choudhury, A. Datta, and S. Poddar, “The Electroweak Sector of the pMSSM in the Light of LHC - 8 TeV and Other Data,” *JHEP* **07** (2014) 019, [arXiv:1404.4841 \[hep-ph\]](#).
- [28] T. Han, Z. Liu, and S. Su, “Light Neutralino Dark Matter: Direct/Indirect Detection and Collider Searches,” *JHEP* **08** (2014) 093, [arXiv:1406.1181 \[hep-ph\]](#).
- [29] M. Cahill-Rowley, R. Cotta, A. Drlica-Wagner, S. Funk, J. Hewett, A. Ismail, T. Rizzo, and M. Wood, “Complementarity of dark matter searches in the phenomenological MSSM,” *Phys. Rev. D* **91** no. 5, (2015) 055011, [arXiv:1405.6716 \[hep-ph\]](#).
- [30] B. Bhattacharjee, A. Chakraborty, and A. Choudhury, “Status of the MSSM Higgs sector using global analysis and direct search bounds, and future prospects at the High Luminosity LHC,” *Phys. Rev. D* **92** no. 9, (2015) 093007, [arXiv:1504.04308 \[hep-ph\]](#).
- [31] G. Belanger, D. Ghosh, R. Godbole, and S. Kulkarni, “Light stop in the MSSM after LHC Run 1,” *JHEP* **09** (2015) 214, [arXiv:1506.00665 \[hep-ph\]](#).
- [32] M. Chakraborti, U. Chattopadhyay, A. Choudhury, A. Datta, and S. Poddar, “Reduced LHC constraints for higgsino-like heavier electroweakinos,” *JHEP* **11** (2015) 050, [arXiv:1507.01395 \[hep-ph\]](#).
- [33] K. Hamaguchi and K. Ishikawa, “Prospects for Higgs- and Z-resonant Neutralino Dark Matter,” *Phys. Rev. D* **93** no. 5, (2016) 055009, [arXiv:1510.05378 \[hep-ph\]](#).
- [34] J. Cao, Y. He, L. Shang, W. Su, and Y. Zhang, “Testing the light dark matter scenario of the MSSM at the LHC,” *JHEP* **03** (2016) 207, [arXiv:1511.05386 \[hep-ph\]](#).
- [35] ATLAS Collaboration, G. Aad *et al.*, “Summary of the ATLAS experiment’s sensitivity to supersymmetry after LHC Run 1 — interpreted in the phenomenological MSSM,” *JHEP* **10** (2015) 134, [arXiv:1508.06608 \[hep-ex\]](#).
- [36] E. A. Bagnaschi *et al.*, “Supersymmetric Dark Matter after LHC Run 1,” *Eur. Phys. J. C* **75** (2015) 500, [arXiv:1508.01173 \[hep-ph\]](#).
- [37] A. Choudhury and S. Mondal, “Revisiting the Exclusion Limits from Direct Chargino-Neutralino Production at the LHC,” *Phys. Rev. D* **94** no. 5, (2016) 055024, [arXiv:1603.05502 \[hep-ph\]](#).
- [38] R. K. Barman, B. Bhattacharjee, A. Choudhury, D. Chowdhury, J. Lahiri, and S. Ray, “Current status of MSSM Higgs sector with LHC 13 TeV data,” *Eur. Phys. J. Plus* **134** no. 4, (2019) 150, [arXiv:1608.02573 \[hep-ph\]](#).
- [39] R. K. Barman, G. Belanger, B. Bhattacharjee, R. Godbole, G. Mendiratta, and D. Sengupta, “Invisible decay of the Higgs boson in the context of a thermal and nonthermal relic in MSSM,” *Phys. Rev. D* **95** no. 9, (2017) 095018, [arXiv:1703.03838 \[hep-ph\]](#).
- [40] M. Abdughani, L. Wu, and J. M. Yang, “Status and prospects of light bino–higgsino dark matter in natural SUSY,” *Eur. Phys. J. C* **78** no. 1, (2018) 4, [arXiv:1705.09164 \[hep-ph\]](#).
- [41] L. Roszkowski, E. M. Sessolo, and S. Trojanowski, “WIMP dark matter candidates and searches—current status and future prospects,” *Rept. Prog. Phys.* **81** no. 6, (2018) 066201, [arXiv:1707.06277 \[hep-ph\]](#).
- [42] G. Pozzo and Y. Zhang, “Constraining resonant dark matter with combined LHC electroweakino searches,” *Phys. Lett. B* **789** (2019) 582–591, [arXiv:1807.01476 \[hep-ph\]](#).
- [43] GAMBIT Collaboration, P. Athron *et al.*, “Combined collider constraints on neutralinos and charginos,” *Eur. Phys. J. C* **79** no. 5, (2019) 395, [arXiv:1809.02097 \[hep-ph\]](#).
- [44] K. Wang and J. Zhu, “Funnel annihilations of light dark matter and the invisible decay of the Higgs boson,” *Phys. Rev. D* **101** no. 9, (2020) 095028, [arXiv:2003.01662 \[hep-ph\]](#).
- [45] R. Kumar Barman, G. Belanger, and R. M. Godbole, “Status of low mass LSP in SUSY,” *Eur. Phys. J. ST* **229** no. 21, (2020) 3159–3185, [arXiv:2010.11674 \[hep-ph\]](#).
- [46] M. Van Beekveld, W. Beenakker, M. Schutten, and J. De Wit, “Dark matter, fine-tuning and $(g - 2)_\mu$ in the pMSSM,” *SciPost Phys.* **11** no. 3, (2021) 049, [arXiv:2104.03245 \[hep-ph\]](#).
- [47] R. K. Barman, G. Bélanger, B. Bhattacharjee, R. M. Godbole, and R. Sengupta, “Is Light Neutralino Thermal Dark Matter in the Phenomenological Minimal Supersymmetric Standard Model Ruled Out?,” *Phys. Rev. Lett.* **131** no. 1, (2023) 011802, [arXiv:2207.06238 \[hep-ph\]](#).
- [48] ATLAS Collaboration, G. Aad *et al.*, “Search for heavy Higgs bosons decaying into two tau leptons with the ATLAS detector using pp collisions at $\sqrt{s} = 13$ TeV,” *Phys. Rev. Lett.* **125** no. 5, (2020) 051801, [arXiv:2002.12223 \[hep-ex\]](#).
- [49] CMS Collaboration, A. M. Sirunyan *et al.*, “Search for supersymmetry in final states with two oppositely charged same-flavor leptons and missing transverse momentum in proton-proton collisions at $\sqrt{s} = 13$ TeV,” *JHEP* **04** (2021) 123, [arXiv:2012.08600 \[hep-ex\]](#).

- [50] **ATLAS** Collaboration, G. Aad *et al.*, “Search for chargino–neutralino pair production in final states with three leptons and missing transverse momentum in $\sqrt{s} = 13$ TeV pp collisions with the ATLAS detector,” *Eur. Phys. J. C* **81** no. 12, (2021) 1118, [arXiv:2106.01676 \[hep-ex\]](#).
- [51] **ATLAS** Collaboration, G. Aad *et al.*, “Search for charginos and neutralinos in final states with two boosted hadronically decaying bosons and missing transverse momentum in pp collisions at $\sqrt{s} = 13$ TeV with the ATLAS detector,” *Phys. Rev. D* **104** no. 11, (2021) 112010, [arXiv:2108.07586 \[hep-ex\]](#).
- [52] **CMS** Collaboration, “Search for electroweak production of charginos and neutralinos at $\sqrt{s} = 13$ TeV in final states containing hadronic decays of WW, WZ, or WH and missing transverse momentum,” [arXiv:2205.09597 \[hep-ex\]](#).
- [53] **ATLAS** Collaboration, G. Aad *et al.*, “Search for invisible Higgs-boson decays in events with vector-boson fusion signatures using 139 fb^{-1} of proton-proton data recorded by the ATLAS experiment,” [arXiv:2202.07953 \[hep-ex\]](#).
- [54] **XENON** Collaboration, E. Aprile *et al.*, “Dark Matter Search Results from a One Ton-Year Exposure of XENON1T,” *Phys. Rev. Lett.* **121** no. 11, (2018) 111302, [arXiv:1805.12562 \[astro-ph.CO\]](#).
- [55] **XENON** Collaboration, E. Aprile *et al.*, “Constraining the spin-dependent WIMP-nucleon cross sections with XENON1T,” *Phys. Rev. Lett.* **122** no. 14, (2019) 141301, [arXiv:1902.03234 \[astro-ph.CO\]](#).
- [56] **PICO** Collaboration, C. Amole *et al.*, “Dark Matter Search Results from the Complete Exposure of the PICO-60 C_3F_8 Bubble Chamber,” *Phys. Rev. D* **100** no. 2, (2019) 022001, [arXiv:1902.04031 \[astro-ph.CO\]](#).
- [57] **PandaX-4T** Collaboration, Y. Meng *et al.*, “Dark Matter Search Results from the PandaX-4T Commissioning Run,” *Phys. Rev. Lett.* **127** no. 26, (2021) 261802, [arXiv:2107.13438 \[hep-ex\]](#).
- [58] J. Aalbers *et al.*, “First Dark Matter Search Results from the LUX-ZEPLIN (LZ) Experiment,” [arXiv:2207.03764 \[hep-ex\]](#).
- [59] **PandaX** Collaboration, Z. Huang *et al.*, “Constraints on the axial-vector and pseudo-scalar mediated WIMP-nucleus interactions from PandaX-4T experiment,” *Phys. Lett. B* **834** (2022) 137487, [arXiv:2208.03626 \[hep-ex\]](#).
- [60] **XENON** Collaboration, E. Aprile *et al.*, “First Dark Matter Search with Nuclear Recoils from the XENONnT Experiment,” *Phys. Rev. Lett.* **131** no. 4, (2023) 041003, [arXiv:2303.14729 \[hep-ex\]](#).
- [61] A. Djouadi, “The Anatomy of electro-weak symmetry breaking. II. The Higgs bosons in the minimal supersymmetric model,” *Phys. Rept.* **459** (2008) 1–241, [arXiv:hep-ph/0503173](#).
- [62] **ATLAS** Collaboration, G. Aad *et al.*, “Search for squarks and gluinos in final states with jets and missing transverse momentum using 139 fb^{-1} of $\sqrt{s} = 13$ TeV pp collision data with the ATLAS detector,” *JHEP* **02** (2021) 143, [arXiv:2010.14293 \[hep-ex\]](#).
- [63] M. Carena, J. Osborne, N. R. Shah, and C. E. M. Wagner, “Supersymmetry and LHC Missing Energy Signals,” *Phys. Rev. D* **98** no. 11, (2018) 115010, [arXiv:1809.11082 \[hep-ph\]](#).
- [64] K. Olive, “Review of particle physics,” *Chinese Physics C* **38** no. 9, (Aug, 2014) 090001. <https://dx.doi.org/10.1088/1674-1137/38/9/090001>.
- [65] **Particle Data Group** Collaboration, R. L. Workman and Others, “Review of Particle Physics,” *PTEP* **2022** (2022) 083C01.
- [66] **ATLAS** Collaboration, G. Aad *et al.*, “Search for direct stau production in events with two hadronic τ -leptons in $\sqrt{s} = 13$ TeV pp collisions with the ATLAS detector,” *Phys. Rev. D* **101** no. 3, (2020) 032009, [arXiv:1911.06660 \[hep-ex\]](#).
- [67] S. Heinemeyer, W. Hollik, and G. Weiglein, “FeynHiggs: A Program for the calculation of the masses of the neutral CP even Higgs bosons in the MSSM,” *Comput. Phys. Commun.* **124** (2000) 76–89, [arXiv:hep-ph/9812320](#).
- [68] S. Heinemeyer, W. Hollik, and G. Weiglein, “The Masses of the neutral CP - even Higgs bosons in the MSSM: Accurate analysis at the two loop level,” *Eur. Phys. J. C* **9** (1999) 343–366, [arXiv:hep-ph/9812472](#).
- [69] G. Degrandi, S. Heinemeyer, W. Hollik, P. Slavich, and G. Weiglein, “Towards high precision predictions for the MSSM Higgs sector,” *Eur. Phys. J. C* **28** (2003) 133–143, [arXiv:hep-ph/0212020](#).
- [70] M. Frank, T. Hahn, S. Heinemeyer, W. Hollik, H. Rzehak, and G. Weiglein, “The Higgs Boson Masses and Mixings of the Complex MSSM in the Feynman-Diagrammatic Approach,” *JHEP* **02** (2007) 047, [arXiv:hep-ph/0611326](#).
- [71] T. Hahn, S. Heinemeyer, W. Hollik, H. Rzehak, and G. Weiglein, “High-Precision Predictions for the Light CP -Even Higgs Boson Mass of the Minimal Supersymmetric Standard Model,” *Phys. Rev. Lett.* **112** no. 14, (2014) 141801, [arXiv:1312.4937 \[hep-ph\]](#).
- [72] H. Bahl and W. Hollik, “Precise prediction for the light MSSM Higgs boson mass combining effective field theory and fixed-order calculations,” *Eur. Phys. J. C* **76** no. 9, (2016) 499, [arXiv:1608.01880 \[hep-ph\]](#).
- [73] H. Bahl, S. Heinemeyer, W. Hollik, and G. Weiglein, “Reconciling EFT and hybrid calculations of the light MSSM Higgs-boson mass,” *Eur. Phys. J. C* **78** no. 1, (2018) 57, [arXiv:1706.00346 \[hep-ph\]](#).

- [74] H. Bahl, T. Hahn, S. Heinemeyer, W. Hollik, S. Paßehr, H. Rzehak, and G. Weiglein, “Precision calculations in the MSSM Higgs-boson sector with FeynHiggs 2.14,” *Comput. Phys. Commun.* **249** (2020) 107099, [arXiv:1811.09073 \[hep-ph\]](#).
- [75] G. Belanger, F. Boudjema, A. Pukhov, and A. Semenov, “micrOMEGAs: Version 1.3,” *Comput. Phys. Commun.* **174** (2006) 577–604, [arXiv:hep-ph/0405253](#).
- [76] G. Belanger, F. Boudjema, A. Pukhov, and A. Semenov, “MicrOMEGAs 2.0: A Program to calculate the relic density of dark matter in a generic model,” *Comput. Phys. Commun.* **176** (2007) 367–382, [arXiv:hep-ph/0607059](#).
- [77] G. Belanger, F. Boudjema, A. Pukhov, and A. Semenov, “Dark matter direct detection rate in a generic model with micrOMEGAs 2.2,” *Comput. Phys. Commun.* **180** (2009) 747–767, [arXiv:0803.2360 \[hep-ph\]](#).
- [78] G. Belanger, F. Boudjema, P. Brun, A. Pukhov, S. Rosier-Lees, P. Salati, and A. Semenov, “Indirect search for dark matter with micrOMEGAs2.4,” *Comput. Phys. Commun.* **182** (2011) 842–856, [arXiv:1004.1092 \[hep-ph\]](#).
- [79] G. Belanger, F. Boudjema, A. Pukhov, and A. Semenov, “micrOMEGAs_3: A program for calculating dark matter observables,” *Comput. Phys. Commun.* **185** (2014) 960–985, [arXiv:1305.0237 \[hep-ph\]](#).
- [80] G. Belanger, A. Mjallal, and A. Pukhov, “Recasting direct detection limits within micrOMEGAs and implication for non-standard Dark Matter scenarios,” *Eur. Phys. J. C* **81** no. 3, (2021) 239, [arXiv:2003.08621 \[hep-ph\]](#).
- [81] CMS Collaboration, A. M. Sirunyan *et al.*, “A measurement of the Higgs boson mass in the diphoton decay channel,” *Phys. Lett. B* **805** (2020) 135425, [arXiv:2002.06398 \[hep-ex\]](#).
- [82] B. C. Allanach, A. Djouadi, J. L. Kneur, W. Porod, and P. Slavich, “Precise determination of the neutral Higgs boson masses in the MSSM,” *JHEP* **09** (2004) 044, [arXiv:hep-ph/0406166](#).
- [83] S. Heinemeyer, W. Hollik, H. Rzehak, and G. Weiglein, “The Higgs sector of the complex MSSM at two-loop order: QCD contributions,” *Phys. Lett. B* **652** (2007) 300–309, [arXiv:0705.0746 \[hep-ph\]](#).
- [84] S. Borowka, T. Hahn, S. Heinemeyer, G. Heinrich, and W. Hollik, “Renormalization scheme dependence of the two-loop QCD corrections to the neutral Higgs-boson masses in the MSSM,” *Eur. Phys. J. C* **75** no. 9, (2015) 424, [arXiv:1505.03133 \[hep-ph\]](#).
- [85] J. E. Camargo-Molina, B. O’Leary, W. Porod, and F. Staub, “Stability of the CMSSM against sfermion VEVs,” *JHEP* **12** (2013) 103, [arXiv:1309.7212 \[hep-ph\]](#).
- [86] D. Chowdhury, R. M. Godbole, K. A. Mohan, and S. K. Vempati, “Charge and Color Breaking Constraints in MSSM after the Higgs Discovery at LHC,” *JHEP* **02** (2014) 110, [arXiv:1310.1932 \[hep-ph\]](#). [Erratum: JHEP 03, 149 (2018)].
- [87] N. Blinov and D. E. Morrissey, “Vacuum Stability and the MSSM Higgs Mass,” *JHEP* **03** (2014) 106, [arXiv:1310.4174 \[hep-ph\]](#).
- [88] ALEPH, DELPHI, L3, OPAL, SLD, LEP Electroweak Working Group, SLD Electroweak Group, SLD Heavy Flavour Group Collaboration, S. Schael *et al.*, “Precision electroweak measurements on the Z resonance,” *Phys. Rept.* **427** (2006) 257–454, [arXiv:hep-ex/0509008](#).
- [89] HFLAV Collaboration, Y. Amhis *et al.*, “Averages of b -hadron, c -hadron, and τ -lepton properties as of summer 2016,” *Eur. Phys. J. C* **77** no. 12, (2017) 895, [arXiv:1612.07233 \[hep-ex\]](#).
- [90] CMS, LHCb Collaboration, V. Khachatryan *et al.*, “Observation of the rare $B_s^0 \rightarrow \mu^+ \mu^-$ decay from the combined analysis of CMS and LHCb data,” *Nature* **522** (2015) 68–72, [arXiv:1411.4413 \[hep-ex\]](#).
- [91] Belle Collaboration, K. Hara *et al.*, “Evidence for $B^- \rightarrow \tau^- \bar{\nu}$ with a Semileptonic Tagging Method,” *Phys. Rev. D* **82** (2010) 071101, [arXiv:1006.4201 \[hep-ex\]](#).
- [92] P. Bechtle, S. Heinemeyer, O. Stål, T. Stefaniak, and G. Weiglein, “HiggsSignals: Confronting arbitrary Higgs sectors with measurements at the Tevatron and the LHC,” *Eur. Phys. J. C* **74** no. 2, (2014) 2711, [arXiv:1305.1933 \[hep-ph\]](#).
- [93] O. Stål and T. Stefaniak, “Constraining extended Higgs sectors with HiggsSignals,” *PoS EPS-HEP2013* (2013) 314, [arXiv:1310.4039 \[hep-ph\]](#).
- [94] P. Bechtle, S. Heinemeyer, O. Stål, T. Stefaniak, and G. Weiglein, “Probing the Standard Model with Higgs signal rates from the Tevatron, the LHC and a future ILC,” *JHEP* **11** (2014) 039, [arXiv:1403.1582 \[hep-ph\]](#).
- [95] P. Bechtle, O. Brein, S. Heinemeyer, G. Weiglein, and K. E. Williams, “HiggsBounds: Confronting Arbitrary Higgs Sectors with Exclusion Bounds from LEP and the Tevatron,” *Comput. Phys. Commun.* **181** (2010) 138–167, [arXiv:0811.4169 \[hep-ph\]](#).
- [96] P. Bechtle, O. Brein, S. Heinemeyer, G. Weiglein, and K. E. Williams, “HiggsBounds 2.0.0: Confronting Neutral and Charged Higgs Sector Predictions with Exclusion Bounds from LEP and the Tevatron,” *Comput. Phys. Commun.* **182** (2011) 2605–2631, [arXiv:1102.1898 \[hep-ph\]](#).
- [97] P. Bechtle, O. Brein, S. Heinemeyer, O. Stal, T. Stefaniak, G. Weiglein, and K. Williams, “Recent Developments in HiggsBounds and a Preview of HiggsSignals,” *PoS CHARGED2012* (2012) 024, [arXiv:1301.2345 \[hep-ph\]](#).

- [98] P. Bechtle, O. Brein, S. Heinemeyer, O. Stål, T. Stefaniak, G. Weiglein, and K. E. Williams, “HiggsBounds – 4: Improved Tests of Extended Higgs Sectors against Exclusion Bounds from LEP, the Tevatron and the LHC,” *Eur. Phys. J. C* **74** no. 3, (2014) 2693, [arXiv:1311.0055 \[hep-ph\]](#).
- [99] P. Bechtle, S. Heinemeyer, O. Stal, T. Stefaniak, and G. Weiglein, “Applying Exclusion Likelihoods from LHC Searches to Extended Higgs Sectors,” *Eur. Phys. J. C* **75** no. 9, (2015) 421, [arXiv:1507.06706 \[hep-ph\]](#).
- [100] **Planck** Collaboration, N. Aghanim *et al.*, “Planck 2018 results. VI. Cosmological parameters,” [arXiv:1807.06209 \[astro-ph.CO\]](#).
- [101] G. Bélanger, F. Boudjema, A. Goudelis, A. Pukhov, and B. Zaldivar, “micrOMEGAs5.0 : Freeze-in,” *Comput. Phys. Commun.* **231** (2018) 173–186, [arXiv:1801.03509 \[hep-ph\]](#).
- [102] M. Carena, D. Garcia, U. Nierste, and C. E. M. Wagner, “Effective Lagrangian for the $t\bar{b}H^+$ interaction in the MSSM and charged Higgs phenomenology,” *Nucl. Phys. B* **577** (2000) 88–120, [arXiv:hep-ph/9912516](#).
- [103] L. J. Hall, R. Rattazzi, and U. Sarid, “The Top quark mass in supersymmetric SO(10) unification,” *Phys. Rev. D* **50** (1994) 7048–7065, [arXiv:hep-ph/9306309](#).
- [104] J. Guasch, P. Haflinger, and M. Spira, “MSSM Higgs decays to bottom quark pairs revisited,” *Phys. Rev. D* **68** (2003) 115001, [arXiv:hep-ph/0305101](#).
- [105] S. Dawson, C. B. Jackson, and P. Jaiswal, “SUSY QCD Corrections to Higgs-b Production : Is the Δ_b Approximation Accurate?,” *Phys. Rev. D* **83** (2011) 115007, [arXiv:1104.1631 \[hep-ph\]](#).
- [106] S. Kraml, S. Kulkarni, U. Laa, A. Lessa, W. Magerl, D. Proschofsky-Spindler, and W. Waltenberger, “SModelS: a tool for interpreting simplified-model results from the LHC and its application to supersymmetry,” *Eur. Phys. J. C* **74** (2014) 2868, [arXiv:1312.4175 \[hep-ph\]](#).
- [107] F. Ambrogì, S. Kraml, S. Kulkarni, U. Laa, A. Lessa, V. Magerl, J. Sonneveld, M. Traub, and W. Waltenberger, “SModelS v1.1 user manual: Improving simplified model constraints with efficiency maps,” *Comput. Phys. Commun.* **227** (2018) 72–98, [arXiv:1701.06586 \[hep-ph\]](#).
- [108] J. Dutta, S. Kraml, A. Lessa, and W. Waltenberger, “SModelS extension with the CMS supersymmetry search results from Run 2,” *LHEP* **1** no. 1, (2018) 5–12, [arXiv:1803.02204 \[hep-ph\]](#).
- [109] J. Heisig, S. Kraml, and A. Lessa, “Constraining new physics with searches for long-lived particles: Implementation into SModelS,” *Phys. Lett. B* **788** (2019) 87–95, [arXiv:1808.05229 \[hep-ph\]](#).
- [110] F. Ambrogì *et al.*, “SModelS v1.2: long-lived particles, combination of signal regions, and other novelties,” *Comput. Phys. Commun.* **251** (2020) 106848, [arXiv:1811.10624 \[hep-ph\]](#).
- [111] C. K. Khosa, S. Kraml, A. Lessa, P. Neuhuber, and W. Waltenberger, “SModelS Database Update v1.2.3,” *LHEP* **2020** (2020) 158, [arXiv:2005.00555 \[hep-ph\]](#).
- [112] G. Alguero, S. Kraml, and W. Waltenberger, “A SModelS interface for pyhf likelihoods,” *Comput. Phys. Commun.* **264** (2021) 107909, [arXiv:2009.01809 \[hep-ph\]](#).
- [113] G. Alguero, J. Heisig, C. Khosa, S. Kraml, S. Kulkarni, A. Lessa, H. Reyes-González, W. Waltenberger, and A. Wongel, “Constraining new physics with SModelS version 2,” [arXiv:2112.00769 \[hep-ph\]](#).
- [114] D. M. Asner *et al.*, “ILC Higgs White Paper,” in *Community Summer Study 2013: Snowmass on the Mississippi*. 10, 2013. [arXiv:1310.0763 \[hep-ph\]](#).
- [115] F. An *et al.*, “Precision Higgs physics at the CEPC,” *Chin. Phys. C* **43** no. 4, (2019) 043002, [arXiv:1810.09037 \[hep-ex\]](#).
- [116] M. Carena, A. de Gouvea, A. Freitas, and M. Schmitt, “Invisible Z boson decays at e^+e^- colliders,” *Phys. Rev. D* **68** (2003) 113007, [arXiv:hep-ph/0308053](#).
- [117] N. Baro, F. Boudjema, and A. Semenov, “Full one-loop corrections to the relic density in the MSSM: A Few examples,” *Phys. Lett. B* **660** (2008) 550–560, [arXiv:0710.1821 \[hep-ph\]](#).
- [118] N. Baro, F. Boudjema, G. Chalons, and S. Hao, “Relic density at one-loop with gauge boson pair production,” *Phys. Rev. D* **81** (2010) 015005, [arXiv:0910.3293 \[hep-ph\]](#).
- [119] S. Banerjee, F. Boudjema, N. Chakrabarty, and H. Sun, “Relic density of dark matter in the inert doublet model beyond leading order for the low mass region: 4. The Higgs resonance region,” *Phys. Rev. D* **104** (2021) 075005, [arXiv:2101.02170 \[hep-ph\]](#).
- [120] M. Mahdi Altakach, S. Kraml, A. Lessa, S. Narasimha, T. Pascal, and W. Waltenberger, “SModelS v2.3: Enabling global likelihood analyses,” *SciPost Phys.* **15** no. 5, (2023) 185, [arXiv:2306.17676 \[hep-ph\]](#).
- [121] D. Dercks, N. Desai, J. S. Kim, K. Rolbiecki, J. Tattersall, and T. Weber, “CheckMATE 2: From the model to the limit,” *Comput. Phys. Commun.* **221** (2017) 383–418, [arXiv:1611.09856 \[hep-ph\]](#).
- [122] M. P. Giordani, “Beyond the standard model physics at the tevatron,” *Journal of Physics: Conference Series* **53** no. 1,

- (Nov, 2006) 329. <https://dx.doi.org/10.1088/1742-6596/53/1/021>.
- [123] “XGBOOST Documentation.” <https://xgboost.readthedocs.io/en/stable/>.
- [124] “Higgs cross sections for HL-LHC and HE-LHC.” <https://twiki.cern.ch/twiki/bin/view/LHCPhysics/HiggsEuropeanStrategy/>.
- [125] A. Adhikary, N. Chakrabarty, I. Chakraborty, and J. Lahiri, “Probing the $H^\pm W^\mp Z$ interaction at the high energy upgrade of the LHC,” *Eur. Phys. J. C* **81** no. 6, (2021) 554, [arXiv:2010.14547](https://arxiv.org/abs/2010.14547) [hep-ph].
- [126] **Muon g-2** Collaboration, D. P. Aguillard *et al.*, “Measurement of the Positive Muon Anomalous Magnetic Moment to 0.20 ppm,” *Phys. Rev. Lett.* **131** no. 16, (2023) 161802, [arXiv:2308.06230](https://arxiv.org/abs/2308.06230) [hep-ex].
- [127] T. Aoyama *et al.*, “The anomalous magnetic moment of the muon in the Standard Model,” *Phys. Rept.* **887** (2020) 1–166, [arXiv:2006.04822](https://arxiv.org/abs/2006.04822) [hep-ph].
- [128] “The lep susy working group and the aleph, delphi, l3 and opal experiments,” <http://lepsusy.web.cern.ch/lepsusy/Welcome.html>.
- [129] **ALEPH** Collaboration, A. Heister *et al.*, “Search for scalar leptons in e+ e- collisions at center-of-mass energies up to 209-GeV,” *Phys. Lett. B* **526** (2002) 206–220, [arXiv:hep-ex/0112011](https://arxiv.org/abs/hep-ex/0112011).
- [130] **ALEPH** Collaboration, A. Heister *et al.*, “Absolute mass lower limit for the lightest neutralino of the MSSM from e+ e- data at $s^{**}(1/2)$ up to 209-GeV,” *Phys. Lett. B* **583** (2004) 247–263.
- [131] **DELPHI** Collaboration, J. Abdallah *et al.*, “Searches for supersymmetric particles in e+ e- collisions up to 208-GeV and interpretation of the results within the MSSM,” *Eur. Phys. J. C* **31** (2003) 421–479, [arXiv:hep-ex/0311019](https://arxiv.org/abs/hep-ex/0311019).
- [132] **L3** Collaboration, P. Achard *et al.*, “Search for scalar leptons and scalar quarks at LEP,” *Phys. Lett. B* **580** (2004) 37–49, [arXiv:hep-ex/0310007](https://arxiv.org/abs/hep-ex/0310007).
- [133] **OPAL** Collaboration, G. Abbiendi *et al.*, “Search for anomalous production of dilepton events with missing transverse momentum in e+ e- collisions at $s^{**}(1/2) = 183$ -Gev to 209-GeV,” *Eur. Phys. J. C* **32** (2004) 453–473, [arXiv:hep-ex/0309014](https://arxiv.org/abs/hep-ex/0309014).
- [134] P. Arias, N. Bernal, A. Herrera, and C. Maldonado, “Reconstructing Non-standard Cosmologies with Dark Matter,” *JCAP* **10** (2019) 047, [arXiv:1906.04183](https://arxiv.org/abs/1906.04183) [hep-ph].